Southeastern Geology: Volume 44, No. 3 October 2006

Editor in Chief: S. Duncan Heron, Jr.

Abstract

Academic journal published quarterly by the Department of Geology, Duke University.

SOUTHEASTERN GEOLOGY

12° BEND IN THE EAST COAST FAULT SYSTEM (ECFS): CAUSE OF THE 1886 CHARLESTON, SC, EARTHQUAKE?

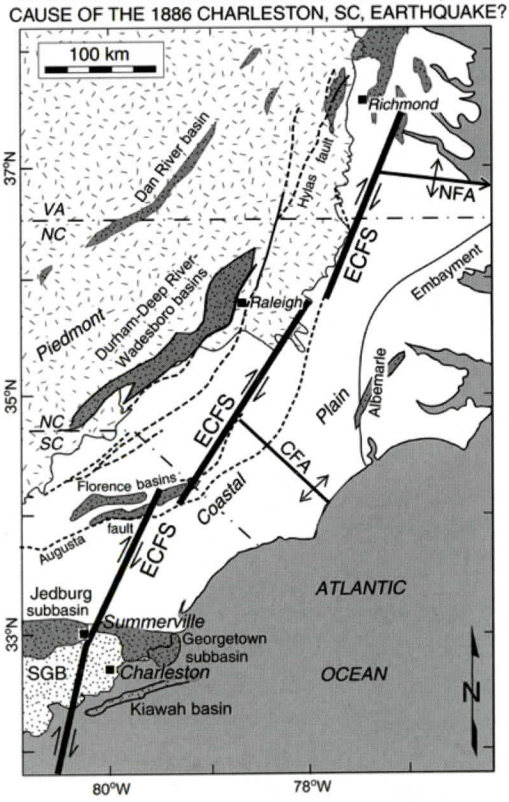

Vol. 44, No. 3 October 2006

SOUTHEASTERN GEOLOGY

PUBLISHED

at

DUKE UNIVERSITY

Duncan Heron

Editor in Chief

David M. Bush

Editor

This journal publishes the results of original research on all phases of geology, geophysics, geochemistry and environmental geology as related to the Southeast. Send manuscripts to **David Bush, Department of Geosciences, University of West Georgia, Carrollton, Georgia 30118, for Fed-X, etc. 1601 Maple St.,** Phone: 678-839-4057, Fax: 678-839-4071, Email: dbush@westga.edu. Please observe the following:

1) Type the manuscript with double space lines and submit in duplicate, or submit as an Acrobat file attached to an email.
2) Cite references and prepare bibliographic lists in accordance with the method found within the pages of this journal. Data citations examples can be found at http://www.geoinfo.org/TFGeosciData.htm
3) Submit line drawings and complex tables reduced to final publication size (no bigger than 8 x 5 3/8 inches).
4) Make certain that all photographs are sharp, clear, and of good contrast.
5) Stratigraphic terminology should abide by the North American Stratigraphic Code (American Association Petroleum Geologists Bulletin, v. 67, p. 841-875).
6) Email Acrobat (pdf) submissions are encouraged.

Subscriptions to *Southeastern Geology* for volume 44 are: individuals - $24.00 (paid by personal check); corporations and libraries - $35.00; foreign $45. Inquires should be sent to: **SOUTHEASTERN GEOLOGY, DUKE UNIVERSITY, DIVISION OF EARTH & OCEAN SCIENCES, BOX 90233, DURHAM, NORTH CAROLINA 27708-0233**. Make checks payable to: *Southeastern Geology*.

Information about **SOUTHEASTERN GEOLOGY** is on the World Wide Web including a searchable author-title index 1958-2001 (Acrobat format). The URL for the Web site is: http://www.southeasterngeology.org

SOUTHEASTERN GEOLOGY is a peer review journal.

ISSN 0038-3678

SOUTHEASTERN GEOLOGY

Table of Contents

Volume 44, No. 3 October 2006

SOUTHEASTERN GEOLOGY
V. 44, No. 3, October 2006, p. 101-127

ASSOCIATION OF THE 1886 CHARLESTON, SOUTH CAROLINA, EARTHQUAKE AND SEISMICITY NEAR SUMMERVILLE WITH A 12° BEND IN THE EAST COAST FAULT SYSTEM AND TRIPLE-FAULT JUNCTIONS

RONALD MARPLE

5041 Alabama Street, Apt 23
El Paso, Texas 79930

RICHARD MILLER

Kansas Geological Survey
1930 Constant Avenue
University of Kansas
Lawrence, Kansas 66047-3726

ABSTRACT

Seismic-reflection data were integrated with other geophysical, geologic, and seismicity data to better determine the location and nature of buried faults in the Charleston, South Carolina, region. Our results indicate that the 1886 Charleston, South Carolina, earthquake and seismicity near Summerville are related to local stresses caused by a 12° bend in the East Coast fault system (ECFS) and two triple-fault junctions. One triple junction is formed by the intersection of the northwest-trending Ashley River fault with the two segments of the ECFS north and south of the bend. The other triple junction is formed by the intersection of the northeast-trending Summerville fault and a newly discovered northwest-trending Berkeley fault with the ECFS about 10 km north of the bend. The Summerville fault is a northwest-dipping border fault of the Triassic-age Jedburg basin that is undergoing reverse-style reactivation. This reverse-style reactivation is unusual because the Summerville fault parallels the regional stress field axis, suggesting that the reactivation is from stresses applied by dextral motion on the ECFS. The southwest-dip and reverse-type motion of the Berkeley fault are interpreted from seismicity data and a seismic-reflection profile in the western part of the study area. Our results also indicate that the East Coast fault system is a Paleozoic basement fault and that its reactivation since early Mesozoic time has fractured through the overlying allochthonous terranes.

INTRODUCTION

The 1886 Charleston, South Carolina, earthquake was the largest eastern U.S. earthquake in historical times (M_w 7.3, Johnston, 1996). It caused heavy damage to most buildings in Charleston and Summerville and produced widespread liquefaction and ground deformation, such as horizontal flexures, within the meizoseismal area (Dutton, 1890; Nuttli and others, 1986; Peters and Herrmann, 1986) (Figure 1).

Because of the controversy surrounding its cause, several tectonic models have been proposed to explain the Charleston earthquake. Seeber and Armbruster (1981), for example, proposed that it was associated with backslip on the Appalachian décollement. Behrendt (1983) proposed that movement on a northeast trending listric fault near the southeast edge of the Triassic-age Jedburg basin may have caused the earthquake. Talwani (1986), in contrast, postulated that the Charleston earthquake and Summerville area seismicity are from stresses produced by the intersection of the north-northeast-trending Woodstock fault and the northwest-trending Ashley River fault (Figure 2A). The Woodstock fault is defined from seismicity as a right-lateral strike-slip fault dipping steeply to the west while the northwest-trending Ashley

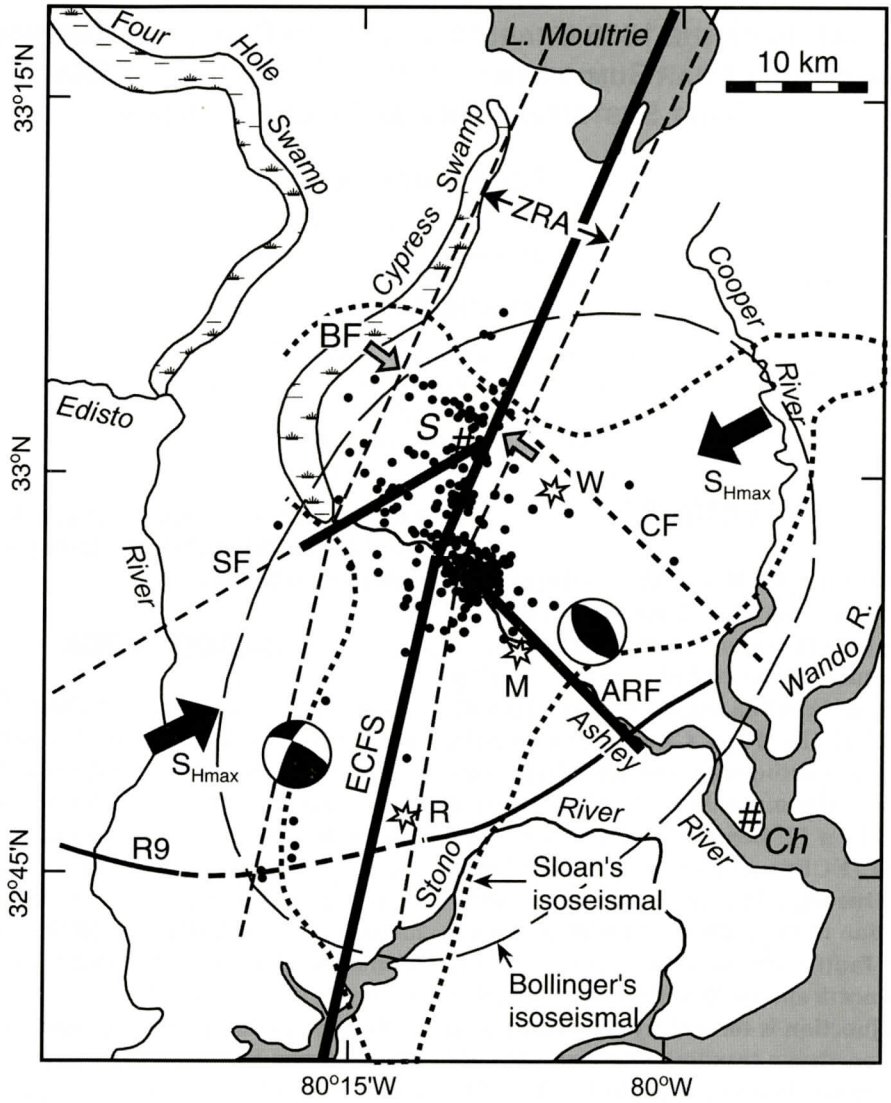

Figure 1. Summary map showing various known features in the Charleston area. The MMI X isoseismal contour of Bollinger (1977) (thin dashed oval contour) shows the approximate location of the meizoseismal area of the 1886 Charleston earthquake. The East Coast fault system (ECFS) is delineated by thick black line. Black dots represent small earthquakes between 1974 and 2003. Generalized focal mechanism solutions are shown for the seismically-defined Woodstock (WF, southern end of ECFS) and Ashley River faults (thick black line denoted ARF). Compressional quadrants are shaded. The three stars delineate the three epicenters for the 1886 earthquake (in order of occurrence: W, Woodstock; R, Ravenel; M, Middleton Place; from Dutton, 1890; Talwani, 1999). The location of the Charleston fault (CF) is estimated from Lennon (1986) and SF is the Summerville fault (dashed where inferred). The Berkeley fault (BF) lies between the open arrows. Uplifted part of releveling line 9 (denoted R9) from Poley and Talwani (1986) is dashed. Northeast-trending, parallel dashed lines denote the location of the zone of river anomalies (ZRA) of Marple and Talwani (2000). Solid arrows indicate axis of maximum horizontal compressive stress field (Zoback and Zoback, 1989). Sloan's isoseismal of the 1886 Charleston earthquake is denoted by dashed contour (taken from plate XXVII of Dutton, 1890). Note the absence of seismicity along the southern part of the ECFS that ruptured in 1886. Ch, Charleston; S, Summerville.

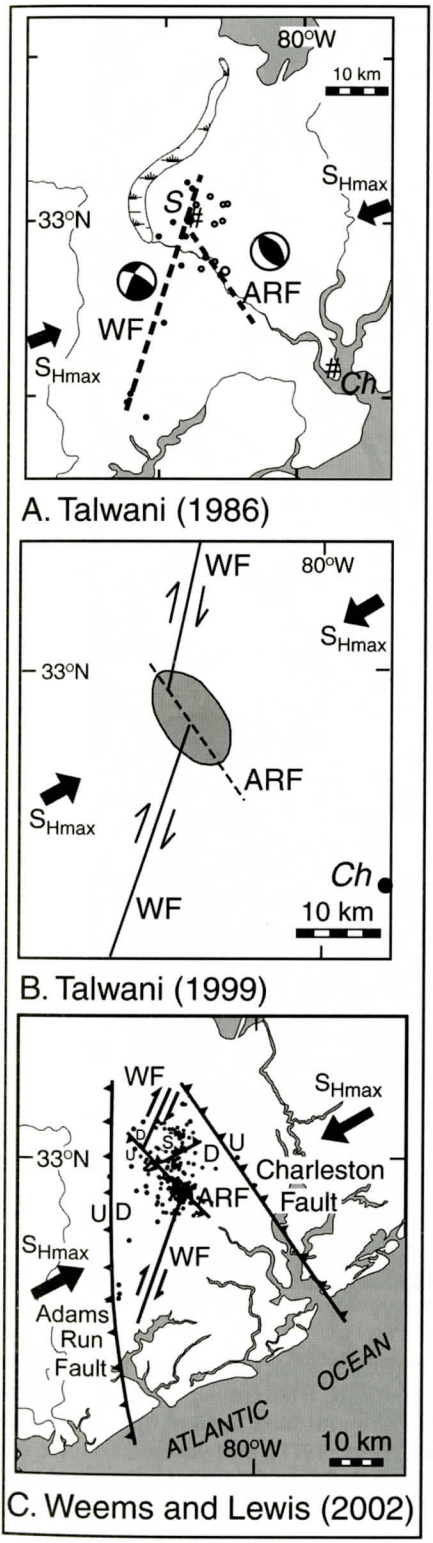

River fault is defined as a reverse fault with up-to-the-southwest motion (e.g., Madabhushi and Talwani, 1993). More recent studies postulated that the Woodstock fault is left-laterally offset about 3-4 km along the Ashley River fault (Garner, 1998; Talwani, 1999; Durá-Gómez, 2004) (Figure 2B). The results of this study argue against this offset.

Based mainly on shallow stratigraphic data, Weems and Lewis (2002) proposed that scissors-like compression on a crustal block between a north-trending Adams Run fault and a northwest-trending Charleston fault controls tectonism in the Charleston area (Figure 2C). The tectonic stress applied by these two hypothetical faults is relieved by displacements on the Woodstock, Summerville, and Ashley River faults, which Weems and Lewis assumed are relatively short faults located between the Adams Run and Charleston faults (Figure 2C). Our results do not support the existence of the Adams Run fault.

In contrast to Weems and Lewis's model, Marple and Talwani (1993; 2000) hypothesized that the seismically-defined Woodstock fault is associated with the southern end of the much longer East Coast fault system (ECFS) (Figure 3). The ECFS is buried by thick Coastal Plain sediments along most of its length, except in central North Carolina where surface faults have been noted. Its crosscutting relationship with allochthonous Alleghanian terranes

Figure 2. Hypothetical models proposed to explain the 1886 Charleston, South Carolina, earthquake and seismicity near Summerville. Diagram A is Talwani's (1986) model in which he postulated that the Charleston earthquake and Summerville area seismicity are from stresses produced by the intersection of the Woodstock (WF) and Ashley River (ARF) faults. In diagram B, stresses associated with the left-lateral offset of the Woodstock fault produced the Charleston earthquake and recent seismicity (Garner, 1998; Talwani, 1999; Durá-Gómez, 2004). Diagram C is Weems and Lewis's (2002) model in which they proposed that tectonism in the Charleston area is controlled by scissors-like compression on a crustal block between two hypothetical faults: the Adams Run and Charleston faults. The tectonic stress applied by these two faults is then relieved by displacements on the Woodstock, Summerville, and Ashley River faults, which they postulated were relatively short structures located between the Adams Run and Charleston faults. Ch, Charleston; S, Summerville.

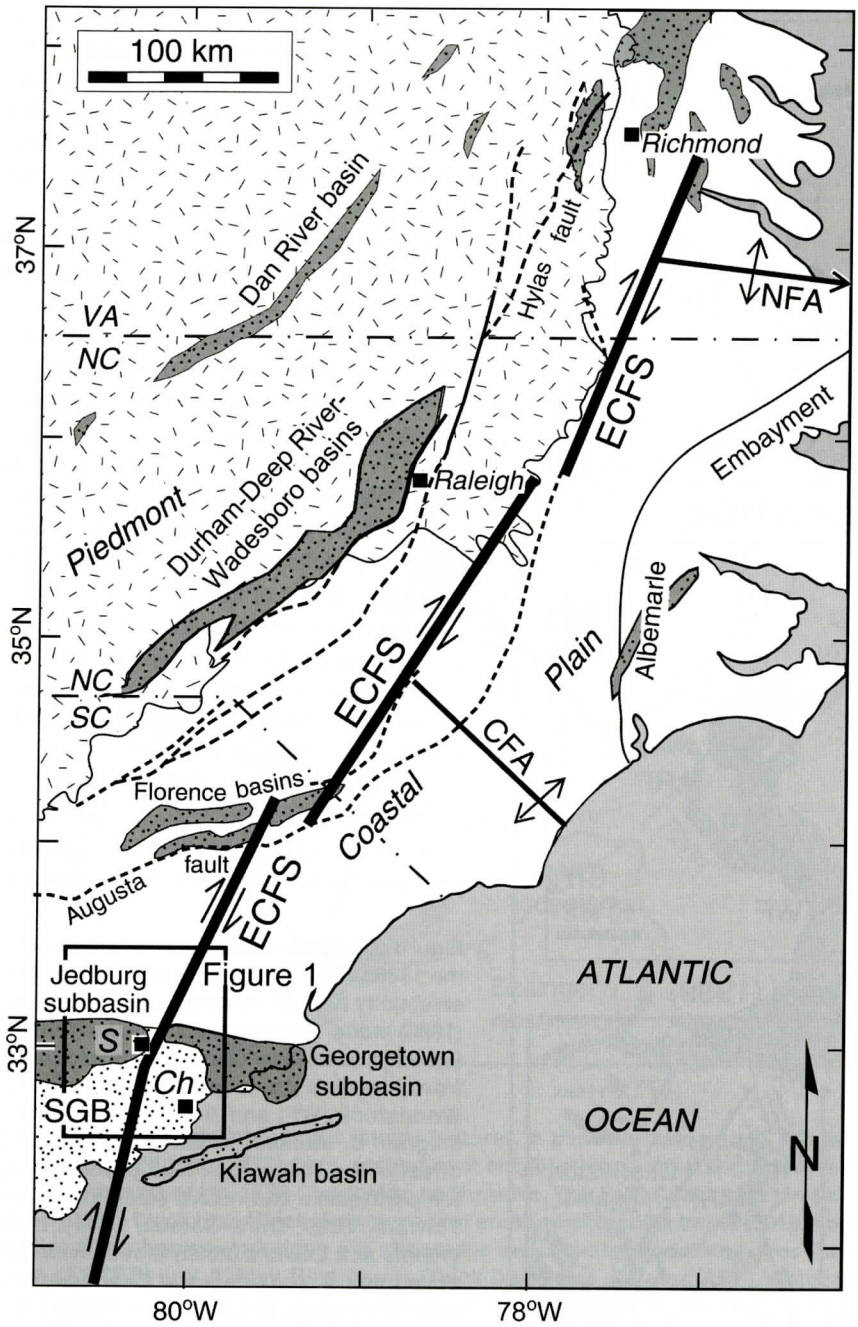

Figure 3. Summary map showing East Coast fault system (ECFS, thick black lines, from Marple and Talwani, 2000), Cape Fear and Norfolk arches (CFA and NFA, from Soller, 1988, and Pazzaglia, 1993), Albemarle embayment (Gohn, 1988), Eastern Piedmont fault system (thin solid and dashed lines in Coastal Plain and Piedmont, Hatcher and others, 1977), and various Triassic rift basins (gray stippled areas, Klitgord and others, 1988). SGB is South Georgia basin. Inset box denotes the location of Figure 1.

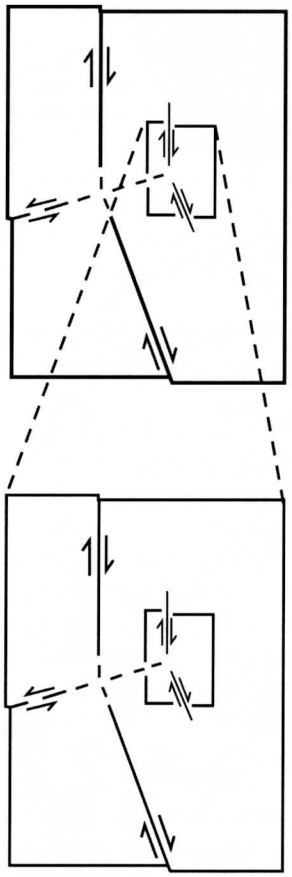

A. Fault bend model of King and Nabelek (1985) .

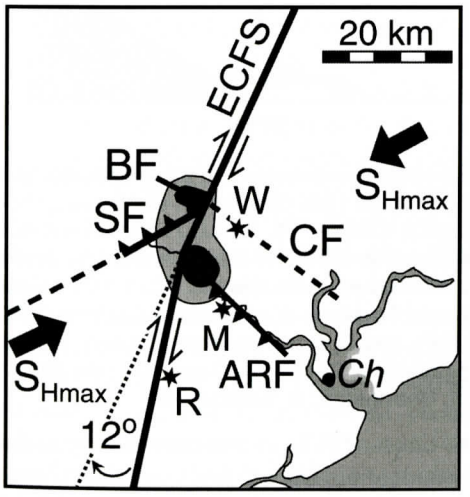

B. Charleston fault bend model.

suggests that it is a basement fault and that its reactivation has fractured through the overlying terranes (e.g., Marple and Talwani, 2004). Our results support this conclusion. Geomorphic and stratigraphic data, studies of paleoliquefaction deposits in South Carolina, and surface faults in central North Carolina indicate that the ECFS has undergone late Cenozoic deformation (e.g., Marple and Talwani, 2000). Marple and Talwani (2004; 2006) hypothesized that the ECFS may be part of an even longer fault system that was offset left-laterally in central Virginia during Alleghanian indention.

The purpose of this study was to reinvestigate the cause of the Charleston earthquake by integrating available seismic-reflection data with seismicity, seismic-refraction, magnetics, stratigraphic, releveling, and geomorphic data. Our results suggest that local stresses caused by a 12° bend in the ECFS and its intersection with the Ashley River, Summerville, and Berkeley faults produced the Charleston earthquake and seismicity near Summerville (Figures 1 and 3). The Ashley River fault intersects the ECFS on the inside (east side) of the bend, but without offsetting the ECFS as suggested in previous models. Based on this observation and previous models of fault bends (e.g., King and Nabelek, 1985), past dextral motion along the ECFS bend likely produced the Ashley River fault (Figure 4). The other two cross-faults, the Summerville

Figure 4. Comparison of the fault bend model of King and Nabelek (1985) (diagram A) with the fault intersections and ECFS bend near Summerville, South Carolina (diagram B). According to King and Nabelek (1985), deformation at a three-fault junction can be accommodated by smaller secondary faults subparallel to the main faults in the upper part of diagram A. These meet at an angle to create yet smaller faults (lower part of diagram A). Note the similarity between King and Nabelek's model and the fault orientations in diagram B. ARF, Ashley River fault; BF, Berkeley fault; CF, Charleston fault; SF, Summerville fault. The three stars delineate the three 1886 epicenters (in order of occurrence: W, Woodstock; R, Ravenel; M, Middleton Place; after Dutton, 1890 and Talwani, 1999). Gray shaded areas near Summerville represent areas of seismicity, darker shading represents greater level of seismicity.

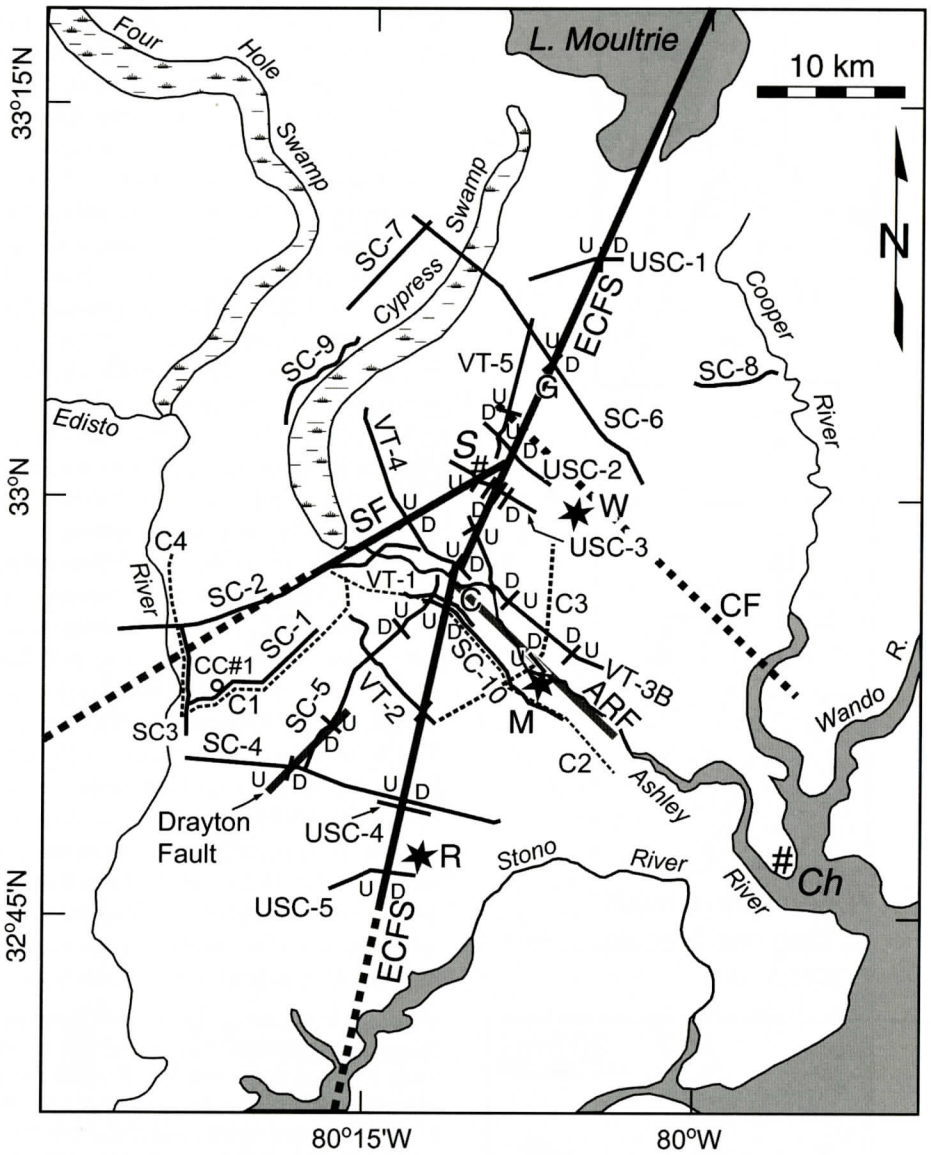

Figure 5. Summary map showing locations of seismic-reflection profiles and inferred faults (U on upthrown side). Solid stars denote the three epicenters of the 1886 Charleston earthquake. Seismic line abbreviations: C, COCORP; SC, U.S. Geological Survey; VT, Virginia Polytechnic Institute and State University; USC, University of South Carolina. COCORP lines denoted by dashed lines and other seismic lines denoted by solid lines. The small circle labeled CC#1 near seismic line SC-1 denotes the location of Clubhouse Crossroads Corehole #1 of Gohn and others (1983). ECFS, Ashley River fault (ARF), Summerville fault (SF), and Drayton fault are denoted by thick gray lines. Charleston fault (CF) denoted by dashed gray line. Cooke (C), Gants (G), and Drayton faults are taken from Hamilton and others (1983). Ch, Charleston; S, Summerville.

and Berkeley faults, intersect the ECFS near Summerville to form a second triple-fault junction along the ECFS. Various data suggest that the Summerville fault, first proposed by Weems and others (1997), is a northwest-dipping border fault of the Jedburg basin and that it has undergone reverse-style reactivation while the Berkeley fault is a northwest-trending, south-

west-dipping, reverse-style fault (Figure 4).

These results are important for various reasons. First, they provide a seismotectonic model that will help to determine the cause of the 1886 earthquake and strain accumulation near Summerville. Secondly, they demonstrate the value of integrating a wide variety of data types when searching for buried active faults with small displacements in intraplate areas.

SEISMIC-REFLECTION STUDIES OF THE MEIZOSEISMAL AREA

Several seismic-reflection studies have been carried out in the meizoseismal area of the Charleston earthquake to search for the causative faults. Various data were acquired by the Kansas Geological Survey (lines abbreviated USC), U.S. Geological Survey (lines abbreviated SC), Virginia Polytechnic Institute and State University (lines abbreviated VT), and the Consortium for Continental Reflection Profiling (COCORP, lines abbreviated C). Only the USC and Virginia Tech seismic-reflection data have not been published. The USC data and part of seismic line VT-2 are presented here. The other VT lines are included in the dissertation of Marple (1994). Figure 5 summarizes the locations of the various surveys used in this study and the faults interpreted from them. Faults interpreted from the VT lines in Figure 5 are taken from Marple (1994).

In 1978, COCORP acquired four 16- and 24-fold Vibroseis seismic-reflection profiles in the meizoseismal area totaling 72 km (Schilt and others, 1983) (Figure 5). Profiles C1, C2, and C4 approximately coincide with USGS lines SC-1, SC-10, and SC-3, respectively. Line C3 was acquired across the Ashley River fault, but with an ~3-km-wide gap at the Ashley River and surrounding swamp. Schilt and others (1983) concluded that a fault exists within this gap because the basement reflection is 0.1 sec two-way travel time (TWTT) lower to the northeast and because diffractions are present on the northeast side of the gap. This up-to-the-southwest sense of displacement is consistent with that of the seismically-defined Ashley River fault, suggesting a causal relationship.

In 1979, the USGS acquired 140 km of Vibroseis multichannel 12-fold seismic-reflection profiles across the meizoseismal area (Hamilton and others, 1983) (Figure 5). Three of these lines (SC-4, SC-6, and SC-10) traverse the main axis of Sloan's isoseismals and the ECFS. Hamilton and others (1983) interpreted two west-side-up faults on lines SC-6 and SC-10, which they named Cooke and Gants faults, respectively (Figure 5). The J reflection, which represents the top of a Jurassic-age basalt flow beneath the Coastal Plain sediments (e.g., Dillon and others, 1979), was offset up-to-the-west about 50 msec TWTT (~50 m) along each of these faults. They further postulated that the Cooke fault continued southwest across the northeast end of line SC-5. Our results, however, suggest that the fault on line SC-10 is part of the ECFS. On line SC-4, they interpreted an ~7-km-wide "zone of missing J" in which the J reflection becomes weak or is missing. They concluded that the western edge of this zone is probably not a fault because the reflection from the top of the crystalline basement (reflector B) appeared continuous across this area. Based on the alignment of these features with faults inferred from the various seismic-reflection lines and a 25-km-long linear magnetic anomaly north of Summerville (Figures 1 and 3), Marple and Talwani (2000) reinterpreted these features on lines SC-4, SC-6, and SC-10 as faults associated with the ECFS. Our results support this interpretation.

The USGS also acquired 450 km of 12-fold marine seismic-reflection data off the South Carolina coast in 1979 using a 3,200-m-long, 64-channel streamer and a tuned airgun array (Figure 6) (Behrendt and Yuan, 1987). From these data, Behrendt and others (1983) identified the northeast-trending Helena Banks fault zone. We used these data to search for offshore extensions of the ECFS and the Ashley River and Charleston faults.

In 1981, Virginia Polytechnic Institute and State University (Virginia Tech) collected 51 km of 24-fold seismic-reflection data in the meizoseismal area using the RGL Vibroseis system (lines abbreviated VT in Figure 5). Although these data are not published, they are in-

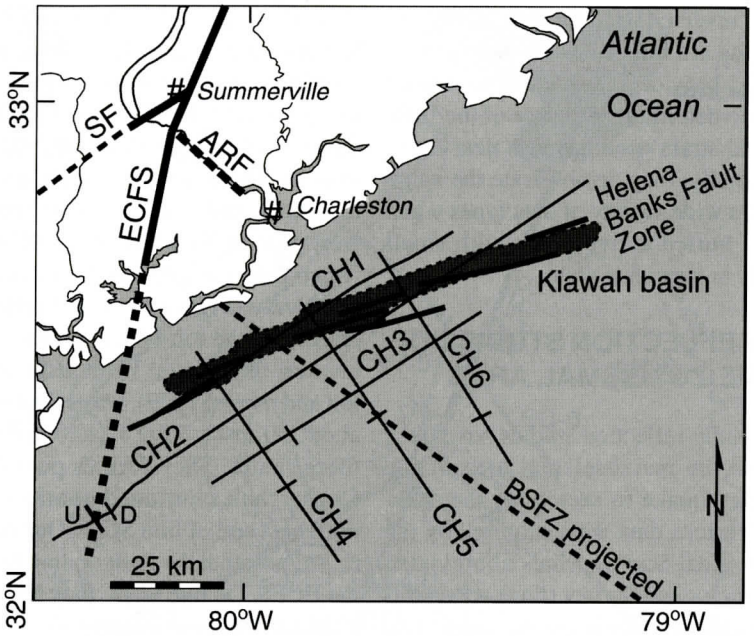

Figure 6. Summary map showing offshore seismic-reflection profiles and interpreted faults (U on upthrown side). Note the up-to-the-west offset on line CH-2 that lines up with the ECFS onshore. Projection of the Blake Spur fracture zone (BSFZ) into study area is denoted by gray dashed line. Kiawah Triassic (?) basin is denoted by gray shaded area surrounded by dashed contour (Behrendt and Yuan, 1987).

cluded as plates in the PhD thesis of Marple (1994). A portion of line VT-2 is included in this study to supplement the few seismic-reflection profiles traversing the ECFS in the southern part of the meizoseismal area.

In 1993, the Kansas Geological Survey acquired five seismic-reflection profiles for the University of South Carolina across the meizoseismal area using two high-resolution methods, the Mini-Sosie and shotgun techniques (lines abbreviated USC on Figure 5). These two techniques are described in the methods section. The purpose of this study was to search for evidence of buried faulting along the trend of the ECFS. In 1996, the Kansas Geological Survey also acquired a 15-km-long Vibroseis profile across the trend of the ECFS 85 km north of Summerville (Marple and Talwani, 2000). These data and a nearby seismic profile acquired by EXXON in 1986 revealed buried faulting along the ECFS. This faulting to the north is significant because it supports the existence of the ECFS well north of the meizoseismal area.

METHODS USED

We combined the previously acquired seismic-reflection data with seismicity, magnetics, seismic-refraction, stratigraphic, and geomorphic data to better determine the location and nature of buried faults in the meizoseismal area of the 1886 earthquake. Acquisition and processing of the USC Mini-Sosie and shotgun seismic-reflection data and their correlation with the local lithostratigraphy are discussed in more detail here.

High Resolution Seismic-Reflection Data

The Mini-Sosie technique is an excellent approach to seismic-reflection data acquisition in a noisy environment because it is acquired at a high enough frequency to allow removal of random noise, such as automobile traffic and bur-

Table 1. Recording and Processing Parameters for USC Profiles

PARAMETER	DESCRIPTION: LINES USC-1, USC-4, USC-5	DESCRIPTION: LINES USC-2, USC-3
Source type	8 gauge auger	3 wackers
Source array	2 m spacing parallel to line	2 m spacing parallel to line
Source duration	1 shot per station	1500 impulses per shot point
Source point interval	16.7 m (55 ft)	16.7 m (55 ft)
Geophone array	Three 40 Hz natural frequency geophones in a cluster, 1 m spacing	Three 40 Hz natural frequency geophones in a cluster, 1 m spacing
Geophone spacing	16.7 m (55 ft)	16.7 m (55 ft)
Line array	48 channels, on-line	24 channels, on-line
Field filters	High cuts 500 Hz, low cuts 25 Hz, 60 Hz notch	High cuts 500 Hz, low cuts 40 Hz, 60 Hz notch
Recording system	EG&G ES 2401	I/O DHR 2400
Sampling rate	0.5 msec	1 msec
Trace length	1 sec	1 sec
Migration velocity	2000 m/sec (1900 m/sec for line USC-5)	2000 m/sec
Polarity	Normal	Normal
CDP range	USC-1: 0-733 USC-4: 0-447 USC-5: 0-800	USC-2: 0-417 USC-3: 0-455
CDPs displayed	USC-1: 200-730 USC-4: 0-447 USC-5: 0-800	USC-2: 25-350 USC-3: 100-350

ied utilities, during processing of the data (Barbier, 1983). The Mini-Sosie method was, therefore, utilized to acquire seismic lines USC-2 and USC-3 where the environment was relatively noisy. The Mini-Sosie technique employs earth compactors as a seismic source, each manually operated by one person.

The other seismic-reflection technique used for the USC study was the shotgun method. It is best used in a relatively noise-free environment due to its lower frequency (Miller and others, 1992). This technique was used to acquire lines USC-1, USC-4, and USC-5 along relatively quiet country roads. It consists of the downhole placement of an 8-gauge shotgun shell in a 0.50-caliber barrel, thereby reducing both the source-generated air-coupled waves and the near-surface material through which the seismic energy must travel. After each shot was recorded, the 48-channel spread and shot location were uniformly moved forward a single-station interval. The two-way travel time recorded for the USC lines was about 1 second (~1 km). See Table 1 for the acquisition parameters.

Data processing was carried out at the Kansas Geological Survey under the supervision of Richard Miller using an Intel 80486-based microcomputer and Eavesdropper software. Stacking velocities were used to determine the approximate depths and thicknesses of the sediments. The velocity functions in general were 1650 m/sec from the surface to 250 msec TWTT, 1850 m/sec from 250 msec to about 600 msec TWTT, and 2050 m/sec from 600 msec to 1000 msec TWTT. Estimations of average velocity, as a function of time and station locations, were made using normal moveout (NMO) curve fitting routines and semblance diagrams averaged across 25 station intervals. Minor statics-related anomalies were removed from the data using surface consistent, elevation, and residual statics corrections. Post-stack migration further improved the signal-to-noise ratio and coherency of the CDP-stacked data. The processing flow is shown in Figure 7.

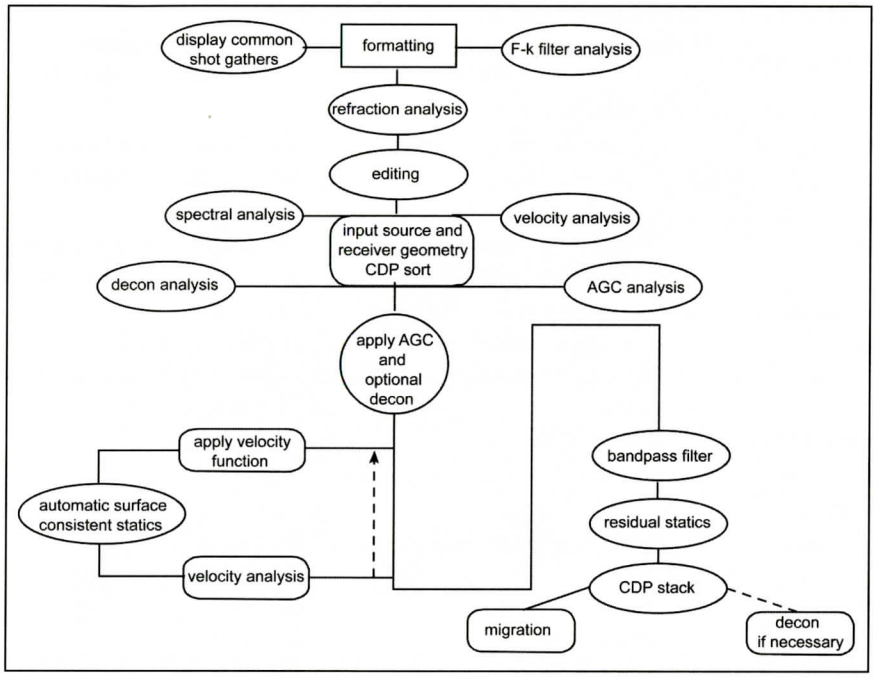

Figure 7. Processing flow used by Kansas Geological Survey for USC seismic-reflection profiles.

Lithostratigraphic Correlations

After data processing was completed, we correlated the data with the local stratigraphy and then examined it for evidence of faulting. Correlations between the USC seismic-reflection data and the lithostratigraphy were based on comparisons between the geologic log of Clubhouse Crossroads Corehole #1 (CC#1, Gohn and others, 1983) and synthetic seismograms produced by Yantis and others (1983) (see Figure 5 for location of CC#1). Four high amplitude reflections were chosen and transferred first to the nearby SC lines and then to the USC lines. The shallowest reflector, labeled T on the seismic-reflection profiles, correlates with an unconformity at the base of the Black Mingo Group (Paleocene-age). A strong reflection of probable Late Cretaceous age and denoted UC corresponds to a large acoustic velocity change at a depth of about 260 m on a continuous velocity log obtained from CC#1. It appears to originate from within the top part of the Peedee Formation (Yantis and others, 1983). Reflector K (Cretaceous age) corresponds to a change from fine quartzose sand to fine quartzose sandy silt, just below the middle of the Cretaceous-age Black Creek Formation. Reflector J represents the top of a Jurassic-age basalt flow encountered at a depth of about 750 m in CC#1. This buried basalt flow is widespread in the Charleston region, covering an area of about 100,000 km^2 (Dillon and others, 1979; Behrendt and others, 1981).

Magnetics Data

The gray-scale aeromagnetic data of Phillips (1988) were instrumental in locating the Summerville fault and the ECFS between Summerville and Lake Moultrie (see Figures 1 and 3 of Phillips, 1988). Flightline spacing was 1 mile (1.6 km) onshore and 2 miles (3.2 km) offshore. Phillips (1988) reduced the data to the pole to center the anomalies and gradients over their sources. He synthetically illuminated these data from the northwest and then performed edge enhancement to highlight structures with northeast trends in the South Carolina Coastal Plain and offshore. He identified several potential geologic structures in the area, but particularly important to this study are the two northeast- to

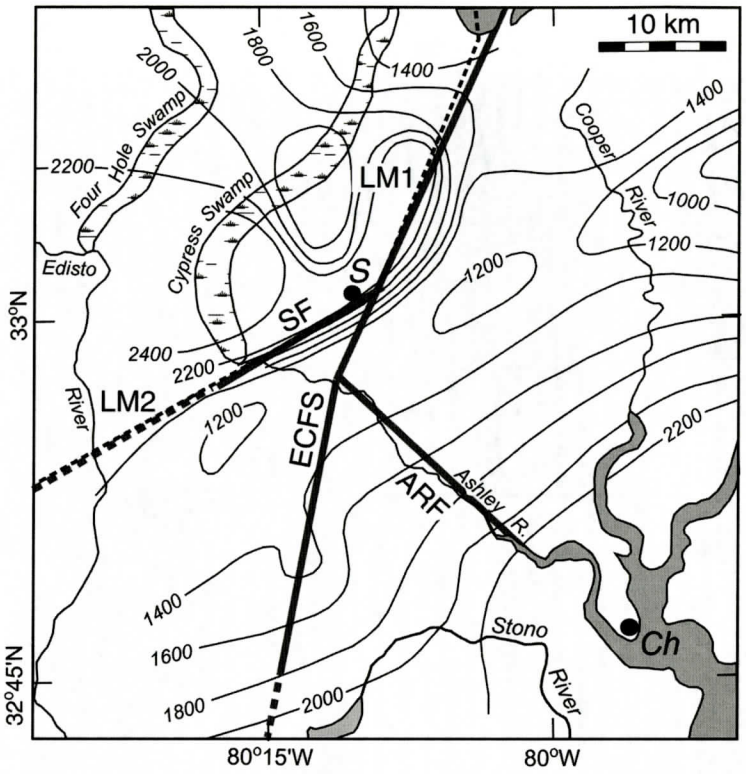

Figure 8. Map comparing ECFS and the Summerville and Ashley River faults (thick gray lines) with elevation contours derived from seismic-refraction interpretation of Ackermann (1983). Contours are meters below sea level of the 6.0- to 6.4-km/s seismic-refracting layer, possibly representing crystalline basement below the Coastal Plain sedimentary wedge. Contour interval is 200 meters. Thin dashed lines labeled LM1 and LM2 are linear magnetic anomalies taken from Phillips (1988). LM1 is nearly coincident with the ECFS. LM2, combined with seismic-reflection, seismic-refraction, and seismicity data, defines the location of the Summerville fault.

north-northeast-trending linear magnetic anomalies near Summerville labeled LM1 and LM2 in Figure 8. Phillips (1988) postulated that the magnetic anomalies are associated with the southeast edge of a subbasin border fault as mapped near Summerville from seismic-refraction data (Amick, 1979; Ackermann, 1983) (Figure 8). Behrendt (1983) named this subbasin the Jedburg basin and postulated that its southeastern border fault may have produced the 1886 Charleston earthquake. The seismic-reflection data presented herein reveals up-to-the-northwest displacement of the highly magnetic Jurassic-age basalt flow (J horizon) and overlying Coastal Plain strata along both of these linear anomalies, suggesting that they are associated with the ECFS and Summerville fault (Figure 5). This up-to-the-northwest displacement contrasts with the down-to-the-northwest displacement of the crystalline basement along this part of the ECFS and eastern border fault. Based on these observations, we postulate that the Summerville fault and the ECFS between Summerville and Lake Moultrie are associated with reverse-style reactivation of the Jedburg basin's southeastern border fault during late Cenozoic time and that the border fault northeast of Summerville was localized by the ECFS during early Mesozoic rifting.

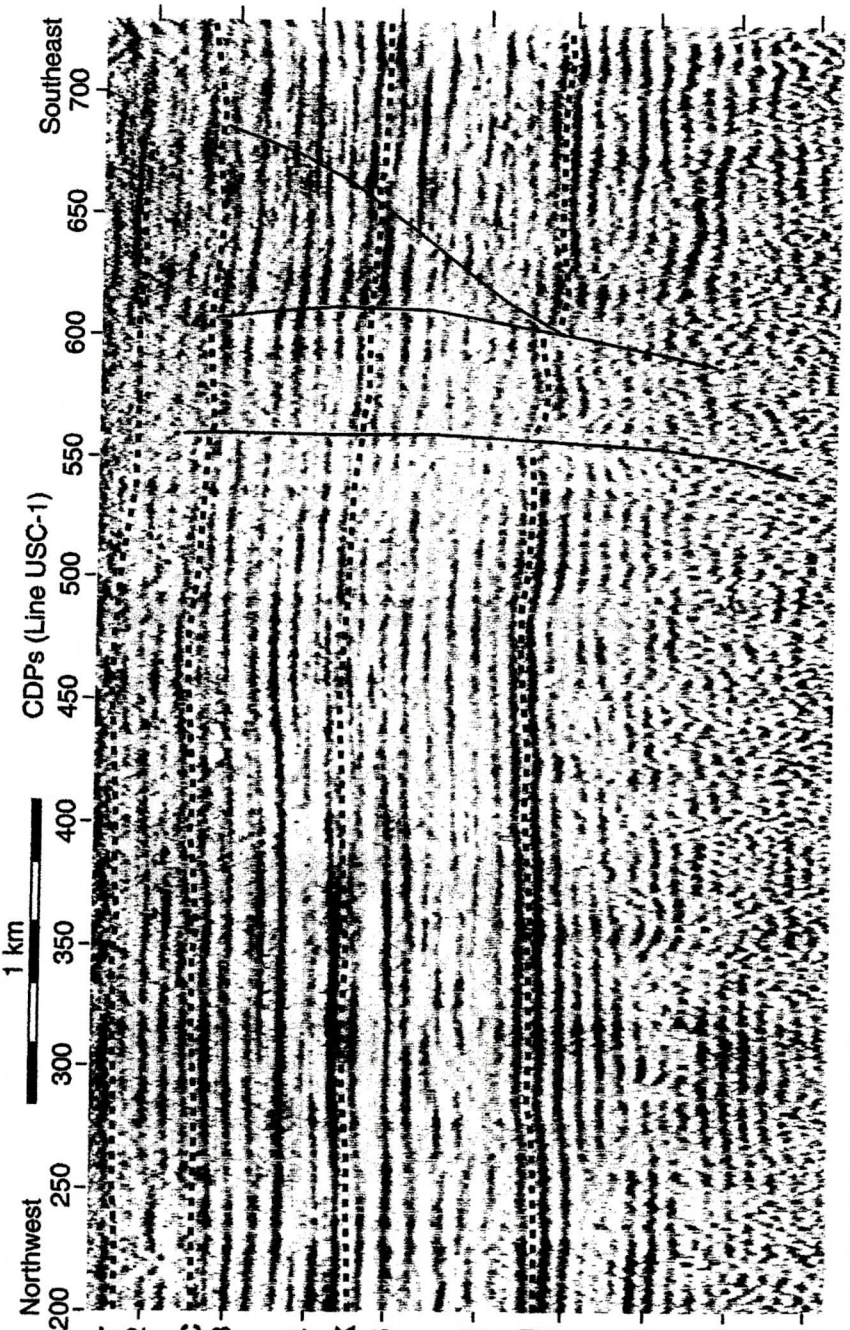

Figure 9. Shotgun seismic-reflection profile USC-1 acquired along Black Tom Bay Road with interpreted west-side-up offsets. T, UC, K, and J represent interpreted horizons (dashed lines, see text for descriptions). Note the gently upwarped reflectors on the upthrown (west) side of the faults. See Figure 5 for location of seismic profile.

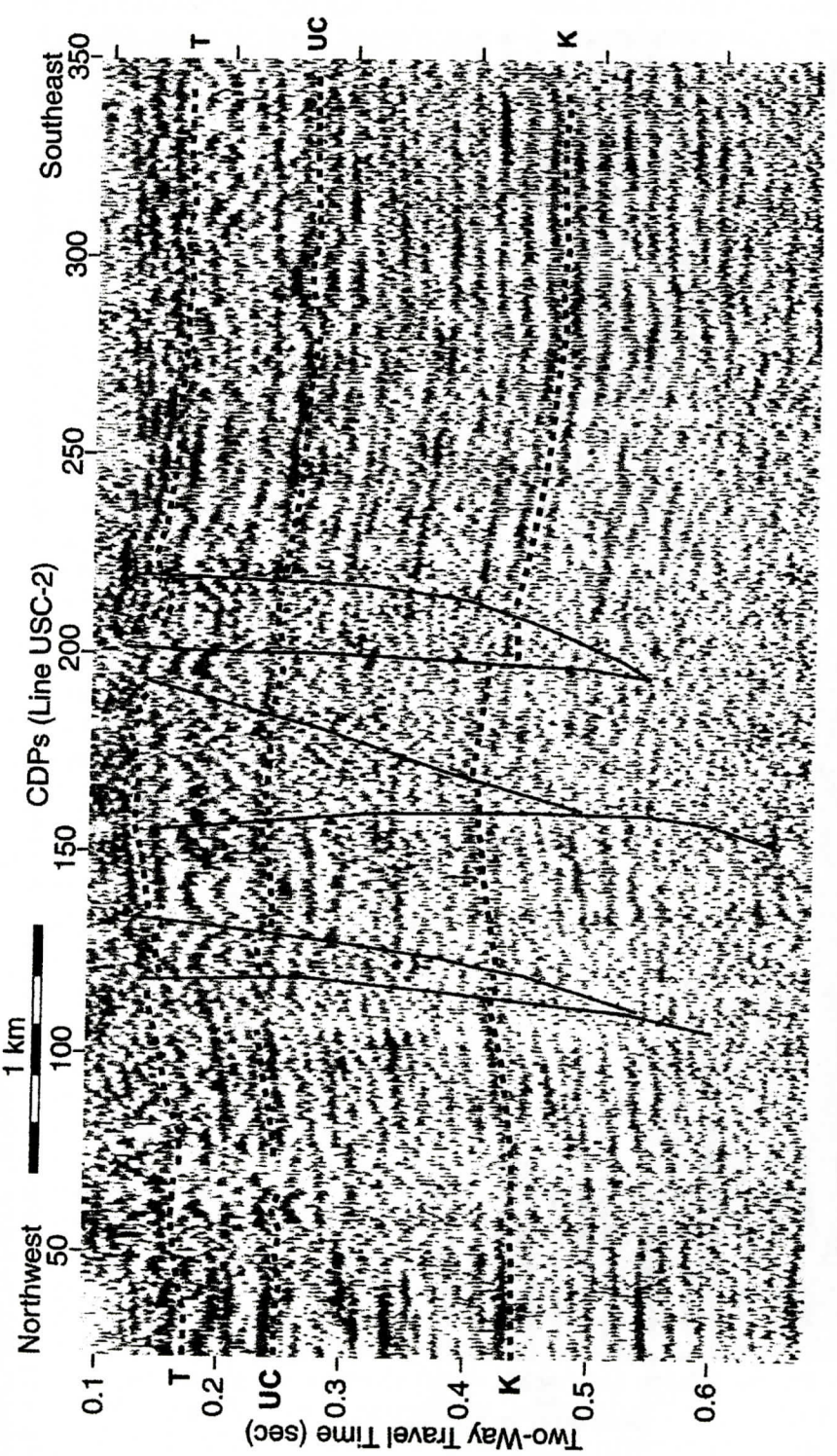

Figure 10. Mini-Sosie seismic-reflection profile USC-2 acquired along Interstate 26 north of Summerville. Note the 1.5 km wide zone of faults with mainly west-side-up offsets and the pronounced upwarping of reflectors near the center of the seismic section. The low signal-to-noise ratio of the data is from high automobile traffic on I-26 during data acquisition. See Figure 5 for location.

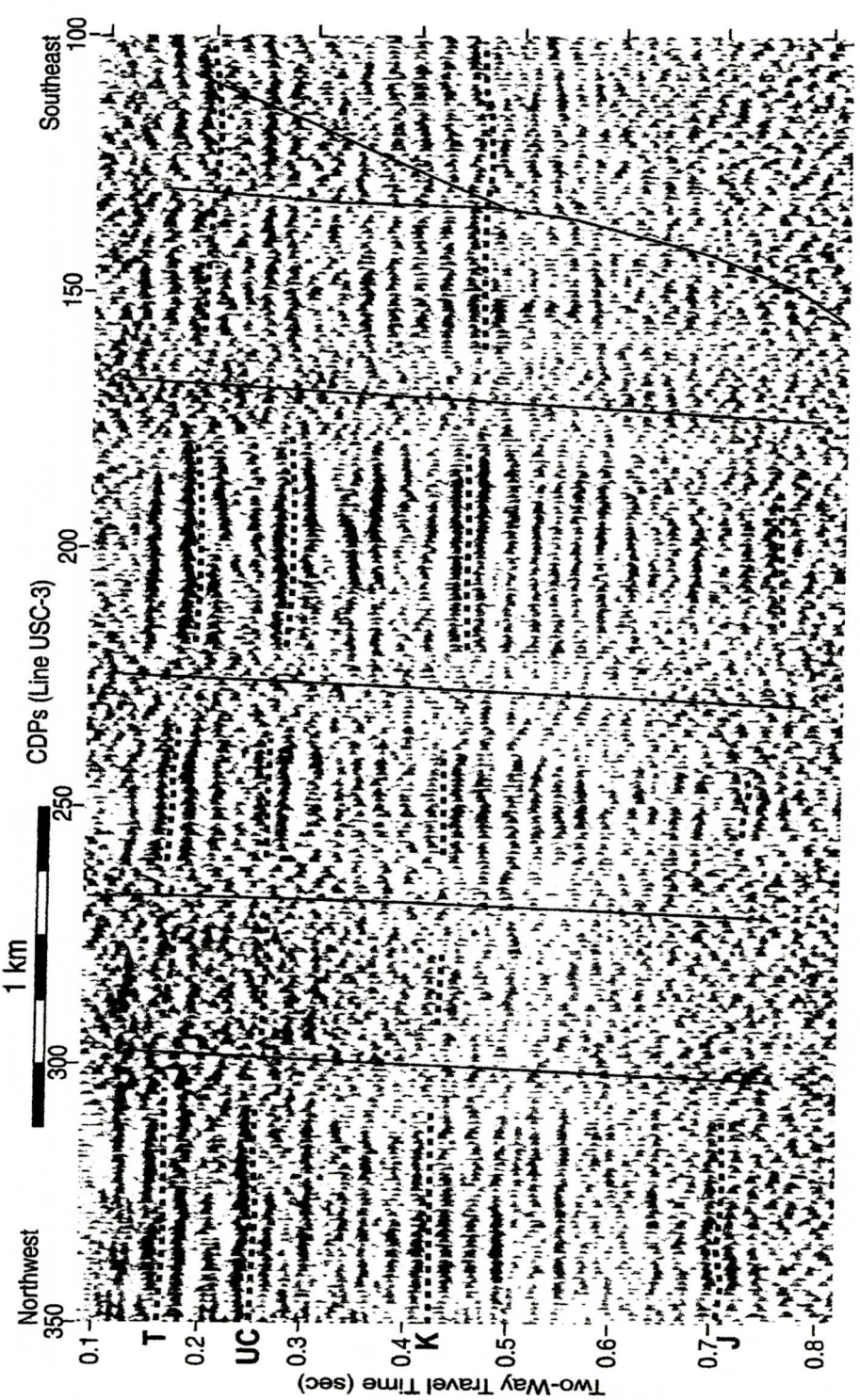

Figure 11. Mini-Sosie seismic-reflection profile USC-3 acquired along Southern Railroad. Note the noncoherent zones and interpreted west-side-up faults. See Figure 5 for location.

INTERPRETATION OF USC SEISMIC-REFLECTION PROFILES AND LINE VT-2

The five USC profiles were acquired across the ECFS trend and were labeled from north to south, USC-1 through USC-5. Line USC-1 was acquired about 14 km north-northeast of Summerville along 5.9 km of Black Tom Bay Road using the shotgun technique (Figure 5). On this profile, reflector J (~500 msec TWTT) is offset up to the west about 30-40 msec along two faults between CDPs 550 and 605 (Figure 9). The offsets diminish upward through the Coastal Plain sedimentary wedge at least to reflector UC. West of these faults, the reflectors are gently upwarped as much as 20 ms TWTT.

Line USC-2 was acquired along 6.7 km of Interstate Highway 26 north of Summerville using the Mini-Sosie method. The low signal-to-noise ratio of these data is due primarily to the heavy volume of traffic that was present during data acquisition. The reflectors from about CDP 120 eastward to about CDP 240 are noticeably upwarped (Figure 10). The upwarping increases with depth and ranges from about 25 msec for reflector T to about 30 msec for reflector K. Also, reflectors T and K are about 20 and 30 msec, respectively, higher on the west end of the profile than on the east side. Several faults between CDPs 120 and 220 offset reflectors through most of the seismic section, forming an ~1.6-km-wide zone. Diffractions are present at about CDP 200 between 130 and 230 msec TWTT. Reflector J, the Jurassic-age basalt flow, is not evident on this line, except for a couple of places along the west side of the profile. This observation is likely from the relatively low amplitudes of the data caused by the relatively low energy transmission of the Mini-Sosie earth compactors.

A second Mini-Sosie profile, line USC-3, was acquired along streets near the Southern Railroad for about 7.3 km through Summerville (Figure 5).The reflectors are relatively flat-lying across the section with small west-side-up offsets at CDPs 170, 225, 268, and 302 (Figure 11). At these CDP locations, the data are characterized by 200-300 m wide zones of noncoherency that extend vertically through the entire section. The largest offset occurs at CDP 225. At this location, the amount of offset ranges from ~30 msec for reflector T to ~50 msec for reflector J. Note that these multiple fault zones occur near the intersection of the Summerville fault and ECFS, suggesting that they represent a highly faulted area near this fault intersection.

A portion of seismic-reflection profile VT-2 shows evidence for strike-slip faulting along the same trend as faults interpreted from the other profiles south of the Ashley River (Figure 5). Deeper reflectors across this line, such as reflectors K and J, are fairly continuous across the entire line, except near CDP 490 (Figure 12).

Table 2. Recording Parameters for Profile VT-2

RECORDING PARAMETER	DESCRIPTION: LINE VT-2
Group interval	35 meters
Near offset	70 meters
Recording instrument	MDS-10
Channels	48
Energy source	Single vibrator, Y-1100
Sweep length	19 sec
Source array	16 X 1 sweeps
Shot interval	35 meters
Far offset	1715 meters
Sample rate	2 msec
Record length	2 sec
Sweep frequency	Down 80-10 Hz
Receiver array	Min-max 20 points
Acquisition date	12/1981

Table 3. Processing Sequence for Line VT-2

Demultiplexing	
Vibroseis whitening and correlation	
Editing	
Static corrections	
Sort/velocity analysis	
Dynamic corrections	
Stacking (24 fold)	
Filtering (15-80 Hz)	
Trace balance	
Polarity - normal	
CDP range:	0-619
CDPs displayed:	395-590

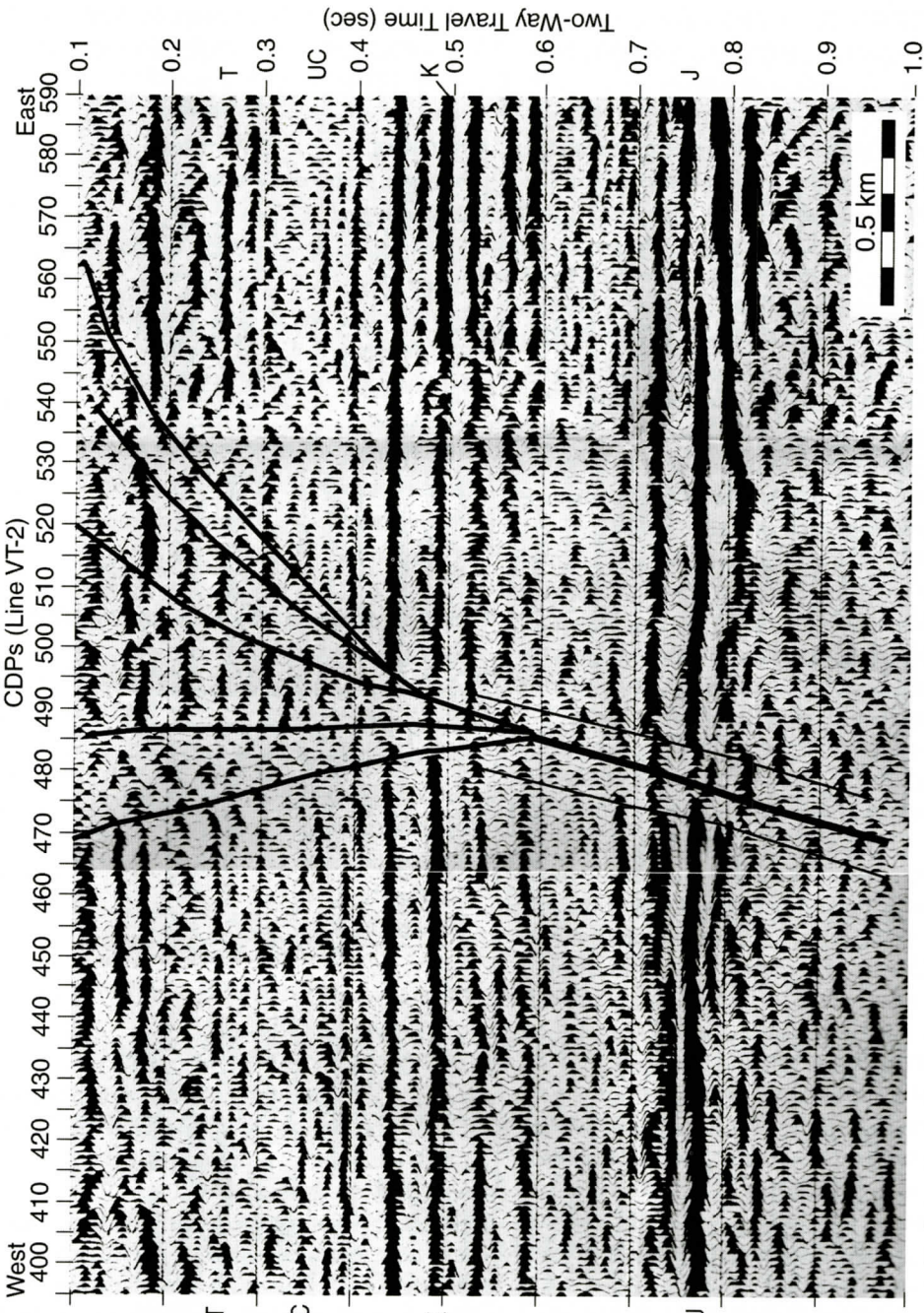

Figure 12. Seismic-reflection profile VT-2. Note the southwest-dipping, ~200-m-wide noncoherent zone in the lower half of the data (between thin black lines) and the palm (flower) structure in the upper half of the data, suggesting transpressional strike-slip faulting. See Figure 5 for location of profile VT-2.

Here, there is an ~200-m-wide zone dipping steeply to the west below about 440 ms TWTT. Although there is little or no vertical displacement within this zone, the reflectors here are distorted and noncoherent, suggesting faulting. The pattern of reflectors in the upper half of the data reveals a palm (flower) structure extending through the entire upper seismic section. Palm structures are commonly associated with transpressional strike-slip faults (Harding, 1985; Naylor and others, 1986). This inferred fault zone does not appear to be from either data processing or uncorrected statics because of its dipping nature (e.g., Tucker and Yorston, 1973; Cox, 1999). Tables 2 and 3 include the recording parameters and processing sequence for profile VT-2.

Further south, seismic line USC-4 was acquired along about 3.7 km of line SC-4 using the shotgun technique to search for evidence of faulting at the western edge of the "zone of missing J" (Figure 5). This location corresponds approximately to CDP 285 on line USC-4. Reflectors on this profile are relatively flat-lying with small offsets (~10 m) at about CDP 285 (Figure 13). Offsets extend upward through nearly the entire seismic section, including reflector T. Diffractions present at about 720 ms and 930 ms TWTT further support the existence of this fault. The pattern of reflections in the upper half of the section also reveals a flower structure, which suggests that this structure is a strike-slip fault. On line SC-4, Hamilton and others (1983) speculated that reflector J may be missing or that the signal becomes weak. On line USC-4, this reflection appears to continue across the section with only a small offset at CDP 285. In contrast, reflection B (top of crystalline basement) is strong west of the fault, but is not discernible to the east, suggesting that it is either downfaulted below the bottom of the seismic section or that its reflection strength is weak to the east. Like reflection B, note that many of the reflectors below reflector K are less discernible east of the fault. The same pattern occurred on line SC-4 across the edge of the "zone of missing J." The reason for this change in amplitude strength is not known, but one possible explanation is that a change in surface material across this zone may have dampened the signal to the east during data acquisition.

Line USC-5 was a shotgun profile that was acquired along part of Old Jacksonboro Road just north of Ravenel (Figures 5 and 14). This is a relatively quiet road in terms of traffic and buried utilities. Toward the center of this profile, between CDPs 220 and 290, is an ~0.5-km-wide, nearly vertical zone that is largely devoid of reflectors, except for a few reflections between 470 and 700 msec TWTT. At this time depth range, the reflector couplets within the noncoherent zone are generally much thinner and in some places interfinger with laterally adjacent reflectors at the edge of the zone, which is suggestive of faulting. The reflectors on either side of this zone are relatively flat-lying, except for a 2-km-wide portion between CDPs 140 and 400. The upwarping is most pronounced in the upper part of the seismic section and appears to be related to a 4-km-wide flower structure. The shallower reflectors down to about 340 msec TWTT along the edges of this zone are upwarped as much as 20 msec TWTT. Deeper in the section, reflector K is offset up-to-the-west ~20 ms across the zone. An arbitrarily selected deeper reflector labeled L was interpreted to help show the increasing vertical offset with depth. It is offset up-to-the-west about 30 ms. Reflector J is not apparent on this profile because of the relatively small amount of energy transmitted by the auger gun. Based on these observations, the noncoherent zone between CDPs 220 and 290 appears to be a nearly vertical zone of intense faulting.

Further south and offshore, a marine seismic-reflection profile (CH-2) traverses the southwest extension of the ECFS (Figure 5) (Behrendt and Yuan, 1987). About 10 km from the southwest end of this profile is a west-side-up Cenozoic fault (Figure 13 of Behrendt and others, 1983) that could be an offshore extension of the ECFS. Deformation is visible as shallow as 0.2 sec TWTT, possibly corresponding to rocks of Eocene age (Behrendt and others, 1983). Behrendt and others (1983) postulated that deformation on this fault occurred during Late Cretaceous time and again in late Cenozoic time.

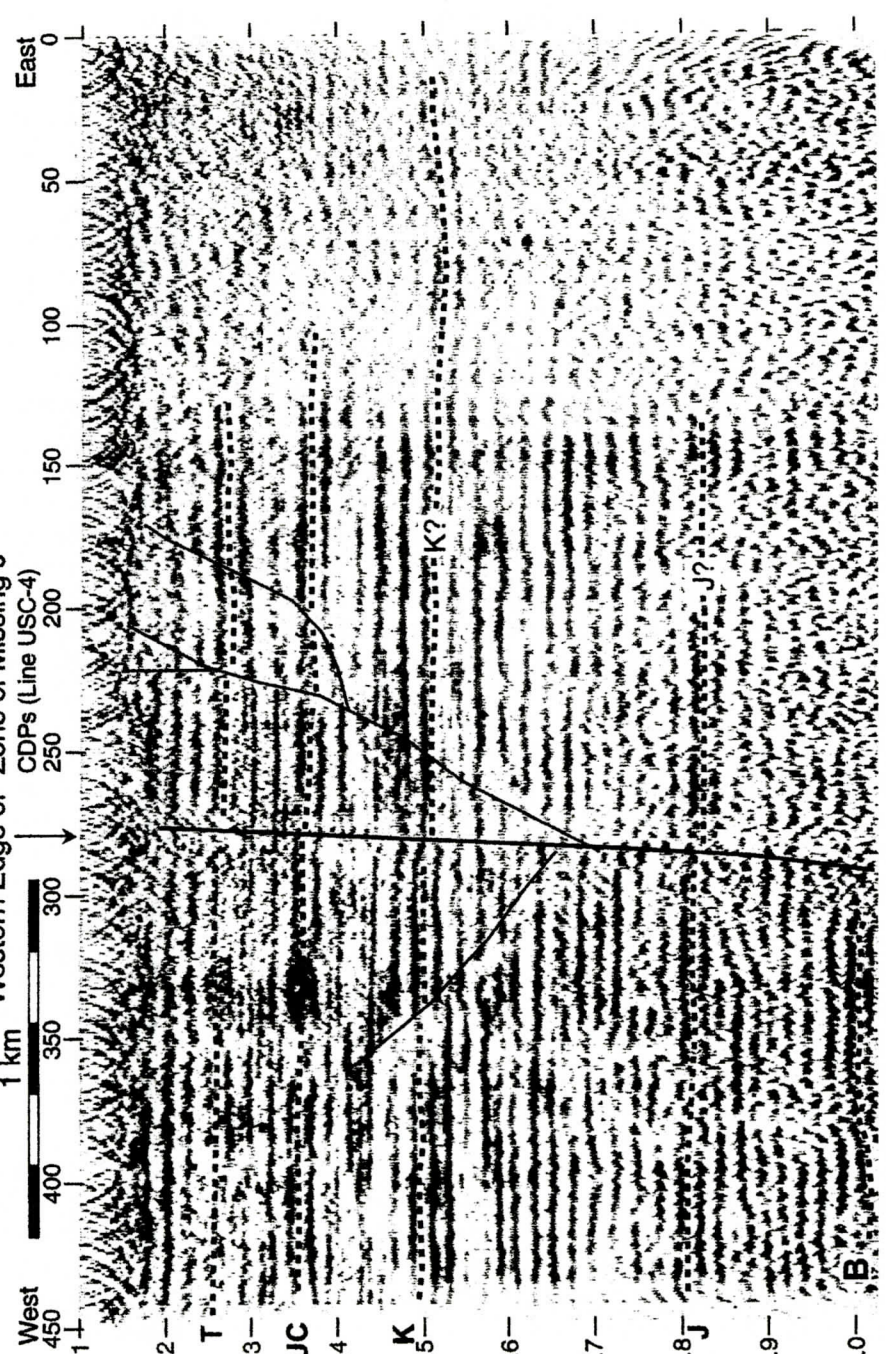

Figure 13. Shotgun seismic-reflection profile USC-4 acquired along part of USGS profile SC-4. Note the near vertical fault and tulip structure branching from the main fault. The main fault coincides with the western edge of the "zone of missing J" on line SC-4 of Hamilton and others (1983). Note the diffractions along the main fault at ~730 and 920 ms TWTT. See Figure 5 for location.

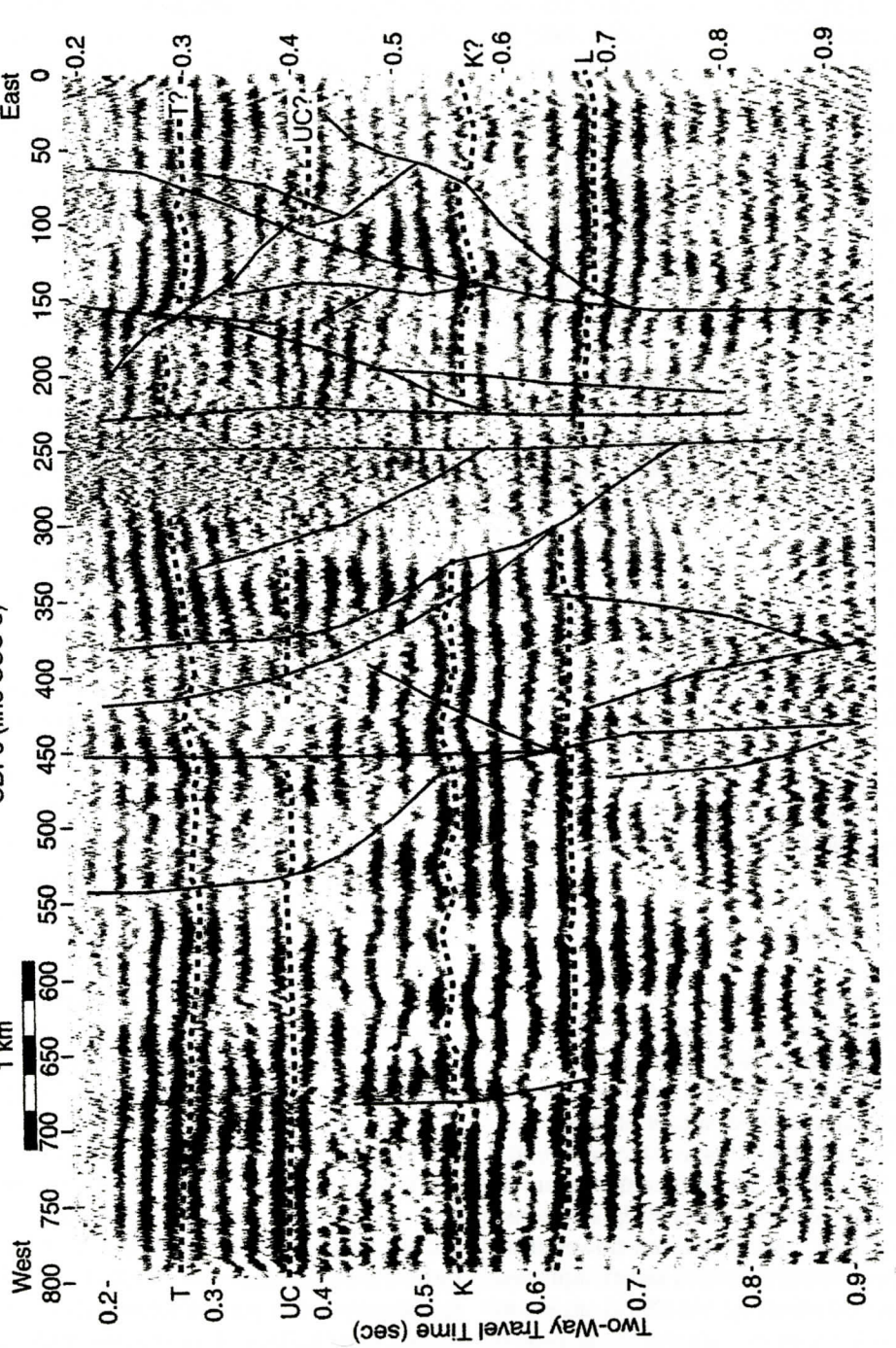

Figure 14. Shotgun seismic-reflection profile USC-5. Note the ~600 m wide noncoherent zone between CDPs 230 and 300 and upwarped sediments above 400 msec TWTT between CDPs 150 and 400. See Figure 5 for location.

Lines VT-3B and VT-4 just north of the Ashley River also revealed Tertiary faults along the trend of the ECFS (Marple, 1994) (Figure 5). Reflector J is offset up-to-the-west ~15 ms along line VT-4. This fault extends upward through the entire seismic section, indicating late Cenozoic deformation. In contrast, reflector J is offset up-to-the-southeast ~20 ms along line VT-3B where it traverses the ECFS trend. This fault also continues upward through the entire seismic section.

DATA INTEGRATION

For the next phase of our study, we integrated the seismic-reflection data with other forms of data to determine the extent and timing of displacements on the ECFS and other faults in the Summerville area. Our results suggest that the ECFS is a major strike-slip fault while other faults traversing the meizoseismal area, such as the Ashley River fault, are limited to the outer Coastal Plain of South Carolina. This integrated study also revealed further evidence for the Summerville fault and led to the discovery of a new, ~6-km-long cross-fault, herein named the Berkeley fault. Here we examine the evidence for each of the Tertiary faults in the Summerville area.

East Coast Fault System (ECFS)

The faults inferred from the seismic-reflection data and a ~40-km-long linear magnetic anomaly between Summerville and Lake Moultrie indicate that the ECFS is relatively continuous in the meizoseismal area with a 12° bend near the Ashley River (Figures 1, 5, and 6). Except for line VT-3B, all profiles showed up-to-the-west displacements along steep, northwest-dipping planes, sometimes with flower structures. These flower structures and multiple fault zones, particularly along line USC-5, are significant because they explain the broad zone of dextral surface flexures observed by Earle Sloan near the Rantowles epicenter (e.g., Plate XXV of Dutton, 1890).

Vertical offsets on the ECFS are noticeably smaller south of Summerville than those to the north (e.g., 30-40 ms vertical offset of reflector J on seismic line USC-1 versus no significant vertical displacement on line VT-2, Figures 9 and 12). This indicates that the ECFS northeast of Summerville has undergone a greater reverse component of dextral-oblique displacement in the past than the ECFS to the south. The small vertical offsets to the south also explain the lack of a linear magnetic anomaly along the ECFS south of Summerville.

Recent deformation on the ECFS is supported mainly from geomorphic, seismicity, and releveling data, much of which have already been discussed by Marple and Talwani (2000). Seismicity near Summerville is the most obvious indication of present deformation on the ECFS. Its proximity to the Ravenel epicenter and the fact that it nearly bisects the main axis of Sloan's isoseismals suggest that the ECFS ruptured south of Summerville in 1886 (Figure 1). The zone of river anomalies (ZRA) along the ECFS indicates that deformation has occurred on the ECFS during late Cenozoic time, not only in the meizoseismal area, but along most of its trend in South Carolina, North Carolina, and Virginia. Another indication of deformation on the ECFS is along its southern end where it coincides with the eastern edge of an area of uplift on releveling line 9 (Figure 15). This uplift is likely from up-to-the-west displacement on the ECFS at depth. Despite this uplift, no seismicity has occurred recently on this part of the fault system. This does not, however, mean that it is no longer active. Faults in other intraplate areas have been intermittently active between periods of little or no deformation, such as those that have produced historic earthquakes in Australia (e.g., Machette and others, 1993), the Bootheel fault in the New Madrid region (Guccione and others, 2005), and the Meers fault in Oklahoma (Crone and Luza, 1990), the latter two of which are aseismic at present. Marple and Talwani (2004) postulated that the lack of seismicity could also mean that this part of the ECFS is currently locked with strain accumulating. Examples of locked, currently aseismic faults that have produced large historic earthquakes include the large segments of the San Andreas fault that

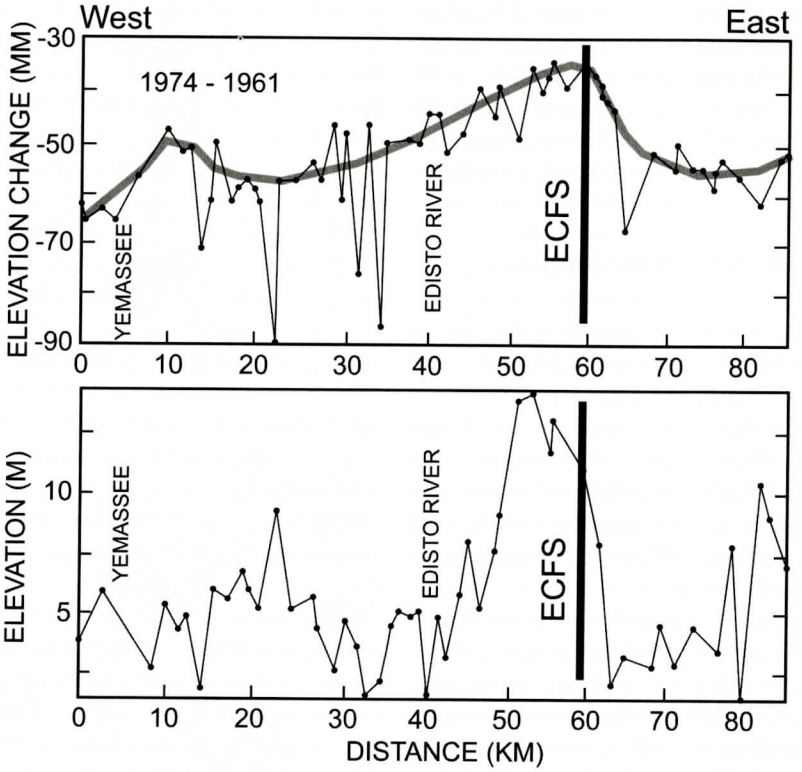

Figure 15. Releveling line 9 showing benchmark elevations (bottom graph) and elevation changes (upper graph) between 1961 and 1974. Location of ECFS is denoted by vertical gray line. Thick gray contour in upper diagram shows average elevation change after removal of elevation spikes interpreted to be erroneous. Modified from Poley and Talwani (1986). Location of releveling line 9 is shown in Figure 1.

ruptured in 1857 and 1906 (Wallace, 1990).

Basement Origin of the ECFS

The localization of the Jedburg basin's eastern border fault along the ECFS between Summerville and Lake Moultrie, the abrupt change in trend of this border fault near Summerville from northeast to north-northeast, and the crosscutting relationship between the ECFS and the Paleozoic allochthonous terranes (Figure 1 of Marple and Talwani, 2000) suggest that the ECFS is a Paleozoic basement fault along which the eastern border fault developed during early Mesozoic rifting. Down-to-the-west normal-sense faulting along this part of the ECFS is indicated by the seismic-refraction results of Ackermann (1983), which show down-to-the-west displacement of the crystalline basement below the Jurassic basalt flow (Figure 8). This is opposite to the relatively small, up-to-the-west Cenozoic displacements on the ECFS above the crystalline basement (Figure 5). The ECFS apparently provided a zone of weakness along which this part of the border fault developed during early Mesozoic rifting. Since early Mesozoic time, the border fault was reactivated in an oblique dextral sense with a reverse component, thus producing the up-to-the-west displacements. The dextral strike-slip motion is based on focal mechanisms, the presence of flower structures along the seismic profiles, and the oblique orientation of the ECFS relative to the axis of the maximum horizontal compressive stress field (Zoback and Zoback, 1989) (e.g., Figures 1, 12, 13, and 14). These observations not only suggest that the ECFS is a Paleozoic basement fault, but that its reactivation since early Mesozoic time has fractured through

the overlying terranes. An example of another large basement fault system overridden by Alleghanian thrusting in the eastern U.S. is the Precambrian basement fault associated with the ~1600-km-long New York–Alabama lineament (King and Zietz, 1978; Johnston and others, 1985).

Ashley River Fault

We found no new evidence for the Ashley River fault because no new seismic-reflection data have been acquired across its trend. Examination of the offshore data indicates that it does not extend offshore and is thus limited to the outer Coastal Plain. It also does not appear to be related to the Blake Spur fracture zone because they are not aligned (Figure 6). Regarding the age of the Ashley River fault, it apparently formed after early Mesozoic rifting because its trend is at a high angle to those of nearby Triassic basins, such as the Kiawah and Jedburg basins (Figures 3 and 6). Its minimum age is Pliocene based on its association with the northwest-trending Fort Bull Bulge and Dome (Weems and Lemon, 1988; Weems and Lewis, 2002).

Charleston and Berkeley Faults

Several studies have speculated on the nature and extent of the Charleston fault (e.g., Lennon, 1986; Weems and Lewis, 2002). Although no seismic-reflection profiles traverse its trend as mapped from corehole data, seismic-reflection profile VT-5 traverses its projection to the northwest. Along this trend, the profile displayed a Tertiary, up-to-the-north, steeply-dipping fault that could be the Charleston fault (Marple, 1994) (Figure 5). The dip direction could not be determined because of the relatively few reflectors on the profile. Displacements were relatively small. Reflector J, for example, was offset about 35 ms TWTT, with offsets decreasing upward through the section. Marple (1994) also noted that reflectors K and J were upwarped about 10 and 15 ms, respectively, for about 2 km on the northeast side of the fault, suggesting compressional deformation. About 2 km to the south is a northwest-elongation of epicenters that could be a downdip representation of this fault. A focal mechanism of one these small earthquakes (solution 50a of Madabhushi and Talwani, 1993) displays southwest-dipping, up-to-the-southwest, reverse-type displacement at about 2.6 km depth (diagram A of Figure 16). The southwest-dipping focal plane is inferred to be the fault plane because its strike parallels the northwest trend of epicenters. Also, its moderate dip projects the fault plane upward approximately to the location of the fault on line VT-5. On the other hand, several observations suggest that the fault defined by the seismicity might not be associated with the fault on profile VT-5 or the Charleston fault. First, the trend defined by the epicenters is more westerly than that for the Charleston fault in Figure 1. Secondly, this trend terminates against the ECFS. Finally, the up-to-the-southwest motion inferred from focal mechanism 50a is opposite the up-to-the-northeast displacement on line VT-5. Because we are uncertain that the fault inferred from the seismicity is related to the Charleston fault, we tentatively refer to it as the Berkeley fault. We also examined the offshore data for evidence of the Charleston fault, but found none (Figure 6). Thus, the Charleston fault appears to be limited to the outer Coastal Plain.

Summerville Fault

Several features support the existence of the Summerville fault first proposed by Weems and others (1997). These features include the alignment of the northeast-trending linear magnetic anomaly southwest of Summerville with an up-to-the-northwest Tertiary fault on seismic line VT-4 (Marple, 1994), focal mechanisms of recent small earthquakes near Summerville (Madabhushi and Talwani, 1993), and a northeast-trending basement fault inferred from the seismic-refraction results of Ackermann (1983) (Figures 1, 5, and 8). Reflector J was offset ~30 ms on line VT-4 and extended upwards through the entire seismic section (Marple, 1994). Diagram B in Figure 16 shows the parallelism between the Summerville fault and the northeast-

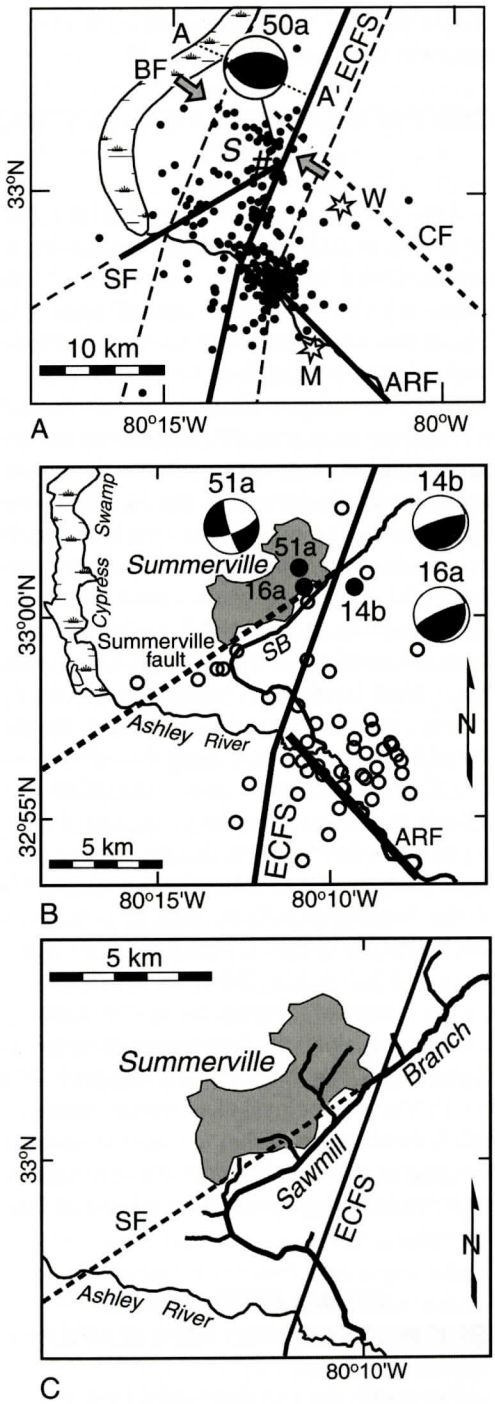

trending focal planes of focal mechanisms 14b (up-to-the-southeast), 16a (up-to-the-southeast), and 51a (left-lateral strike-slip), suggesting a causal association.

Various observations indicate that the Summerville fault is a Triassic normal fault that was reactivated in a reverse sense during late Cenozoic time like that along the ECFS northeast of Summerville. The seismic-refraction results of Schilt and others (1983) suggest that it was part of a down-to-the-northwest listric border fault of the Jedburg basin (Figure 8). In contrast, the Tertiary fault on line VT-4 indicates that the fault was reactivated in an up-to-the-west reverse motion during late Cenozoic time.

Geomorphic and seismicity data suggest that deformation is continuing on the Summerville fault. Several small earthquakes, for example, have been mapped near the fault (Figure 1). The fault also coincides with the northeast-trending part of the Sawmill Branch of the Ashley River (diagram C in Figure 16). Smaller streams draining into the upper Sawmill Branch are unilaterally located on the northwest side of the creek and on the upthrown side of the fault, suggesting that up-to-the-northwest displacement on the Summerville fault may have resulted in the unilateral drainage. Previous studies of drainage systems (e.g., Cox, 1994) support the

Figure 16. Diagrams showing evidence for the northwest-trending Berkeley fault and recent deformation on the Summerville fault (SF). Map A shows the northwest trend of seismicity (solid dots) that defines the Berkeley fault (BF). Note how the strike of the southwest-dipping nodal plane of focal mechanism 50a (line A-A') (Madabhushi and Talwani, 1993) parallels the trend of epicenters. CF, Charleston fault. Map B shows three focal mechanisms (solid dots, 14b, 16a, and 51a from Madabhushi and Talwani, 1993) of small earthquakes with northeast-trending nodal planes that parallel the Summerville fault (SF). Seismicity in map B is denoted by open circles. Seismicity is taken from Madabhushi and Talwani (1993). Map C shows the parallelism between the Summerville fault and the upper reach of Sawmill Branch Creek, and the unilateral drainage on the northwest side of Sawmill Branch, suggesting possible gentle uplift on the northwest side of the Summerville fault.

correlation of unilateral drainage with uplift on the upthrown side of faults. We examined 7.5 minute topographic maps in the area for topographic uplift across the fault trend, but found none. This observation suggests that uplift has been gentle and slow enough for the uplifted area northwest of the Sawmill Branch to be eroded down. These observations, combined with the coincidence of the Summerville and Berkeley faults with the northwest lobe of Sloan's isoseismals, suggest that they may have ruptured after the main shock of the 1886 earthquake (Figure 1).

Stress Loading of the Summerville Fault by the ECFS

An unusual observation regarding the Summerville fault is its parallelism with the axis of maximum horizontal compressive stress and its late Cenozoic reactivation. This orientation does not favor its reverse reactivation by the regional stress field (Sibson, 1990). Thus, it is likely that dextral motion on the nearby ECFS is loading stress on the Summerville fault and causing it to slip.

Adams Run Fault

We examined seismic lines SC-1, SC-2, and SC-4 where they traverse the trend of the proposed Adams Run fault to search for evidence of this fault. These data do not show deformation near the proposed fault, except for the Cretaceous-age Drayton fault on line SC-4 (Hamilton and others, 1983) (Figure 5). This fault, however, has not undergone Cenozoic deformation and appears to trend northeasterly (Hamilton and others, 1983). Thus, the existence of the Adams Run fault is questionable.

Other Unnamed Faults

Two faults were interpreted by Marple (1994) along the southeast half of line VT-3B (Figure 5). Offsets were relatively small, ~15-20 ms on reflector J, but continued upward through the entire seismic section (Marple, 1994). These faults appear to be short faults because they do not continue across nearby seismic lines SC-6, C-2, or SC-10, which approximately parallel line VT-3B.

COMPARISON WITH A FAULT BEND MODEL

According to King and Nabelek (1985), deformation at a three-fault junction can be accommodated by smaller secondary faults subparallel to the main faults (Figure 4A). These meet at an angle creating yet smaller faults (lower part of diagram A of Figure 4). Note the similarity of their model with the fault orientations in Figure 4B. Like King and Nabelek's model, there are smaller north or northeast-trending faults east of the ECFS bend on line VT-3B. The main difference between the two models is that the dominant motion on the Ashley River fault is reverse, rather than strike-slip as in King and Nabelek's model. Based on these observations, we propose that the Ashley River fault formed to compensate for the increased compression and change in volume produced by dextral motion along the ECFS bend. The clustered seismicity east of the ECFS bend reflects the anomalously high amount of stress expected at this location (Figure 1). The other triple-fault junction formed by the intersection of the Summerville fault, Berkeley fault, and the ECFS also bears a strong resemblance to King and Nabelek's (1985) model (Figure 4). Again, note that the greatest concentration of seismicity is along the Berkeley fault northwest of the ECFS, not at the intersection itself (Figure 1). The greater level of seismicity east of the ECFS bend indicates that this area is undergoing greater deformation than the area near the other triple-fault intersection northeast of Summerville.

CONCLUSIONS AND SEISMOTECTONIC IMPLICATIONS

Our results suggest that the ECFS is a major strike-slip fault system in the southeastern U.S. while the Summerville, Ashley River, Charleston, and Berkeley faults are shorter cross-faults limited to the outer Coastal Plain of South Carolina. The 12° bend in the ECFS and intersecting

cross-faults, such as the Charleston and Ashley River faults, are likely responsible for the 1886 Charleston earthquake and recent seismicity near Summerville. The locations of the 1886 epicenters (Figure 1) suggest that oblique-reverse displacement on either the Ashley River or Charleston faults produced the first shock. We, therefore, postulate that a small component of left-lateral displacement may have decreased the normal stress on the ECFS, thus causing it to slip south of the Ashley River. A commonly cited example of this mechanism is the Superstition Hills earthquake of 1987 (e.g., Kahle and others, 1988; Hudnut and others, 1989; Wald and others, 1990). During this earthquake, the Elmore Ranch fault (cross-fault) decreased the normal stress on the Superstition Hills main fault, thus allowing it to rupture.

There is also evidence for late Cenozoic deformation on the ECFS outside the meizoseismal area, though much of its trend is currently aseismic, including the segment south of Summerville that broke in 1886. This lack of seismicity can be explained in several ways: 1) segments that have produced large earthquakes in the past are presently locked with strain accumulating, 2) segments of the ECFS are intermittently active with periods of little or no deformation between moderate to large earthquakes, 3) the ECFS is undergoing aseismic creep, and 4) by the low strain rate in the eastern U.S. Thus, it is important that the ECFS be further investigated to determine if other segments could someday produce large damaging earthquakes like the 1886 event.

In conclusion, this study demonstrates that a gentle 12° bend in a large strike-slip fault system can cause significant strain accumulation and large earthquakes. It also demonstrates the value of combining various data types when mapping buried faults in intraplate areas underlain by a thick sedimentary wedge, especially when little seismicity exists and displacements are relatively small. This is especially true for buried strike-slip faults like the ECFS. Although the ECFS is the major fault system traversing the study area, its vertical offsets are relatively small because of its predominant strike-slip motion and low Cenozoic fault slip rates. These observations, combined with the basement origin of the East Coast fault system and the low level of seismicity along its trend, account for why its identification has been so problematic.

ACKNOWLEDGEMENTS

We thank Cahit Çoruh and John Costain for allowing us to display part of seismic-reflection profile VT-2. Our appreciation is extended to Gered Lennon and an anonymous reveiwer for their critical reading of this manuscript. We are also grateful to the South Carolina Universities Research and Education Foundation for partially funding this research.

REFERENCES CITED

Ackermann, H.D., 1983, Seismic-refraction study in the area of the Charleston, South Carolina, 1886 earthquake, *in* Gohn, G.S., ed., Studies related to the Charleston, South Carolina, earthquake of 1886—Tectonics and seismicity: U.S. Geological Survey Professional Paper 1313-F, 20 p.

Amick, D., 1979, Crustal structure studies in the South Carolina Coastal Plain [M.S. thesis]: University of South Carolina, Columbia, South Carolina, 81 p.

Barbier, M.G., 1983, The Mini-Sosie method, International Human Resources Development Corporation, Houston, 90 p.

Behrendt, J.C., 1983, Did movement on a northeast trending listric fault near the southeast edge of the Jedburg Triassic-Jurassic (?) basin cause the Charleston, South Carolina, 1886 earthquake?, *in* Hays, W.W., and Gori, P.L., eds., Proceedings of Conference XX, A Workshop on the 1886 Charleston, SC, Earthquake and its Implications for Today: U.S. Geological Survey Open File Report 83-843, p. 126-131.

Behrendt, J.C., and Yuan, A., 1987, The Helena Banks strike-slip (?) fault zone in the Charleston, South Carolina, earthquake area: Results from a marine, high-resolution, multichannel, seismic-reflection survey: Geological Society of America Bulletin, v. 98, p. 591-601.

Behrendt, J.C., Hamilton, R.M., Ackermann, H.D., and Henry, V.J., 1981, Cenozoic faulting in the vicinity of the Charleston, South Carolina, 1886 earthquake: Geology, v. 9, p. 117-122.

Behrendt, J.C., Hamilton, R.M., Ackermann, H.D., Henry, V.J., and Bayer, K.C., 1983, Marine multichannel seismic-reflection evidence for Cenozoic faulting and deep crustal structure near Charleston, South Carolina, *in* Gohn, G.S., ed., Studies related to the Charleston, South Carolina, earthquake of 1886—Tectonics and seismic-

ity: U.S. Geological Survey Professional Paper 1313-J, 29 p.

Bollinger, G.A., 1977, Reinterpretation of the intensity data for the 1886 Charleston, South Carolina, earthquake, *in* Rankin, D.W., ed., 1977, Studies related to the Charleston, South Carolina, earthquake of 1886—A preliminary report: U.S. Geological Survey Professional Paper 1028, p. 17-32.

Cox, M.J.G., 1999, Static corrections for seismic reflection surveys: Society of Exploration Geophysicists, Tulsa, Oklahoma, 531 p.

Cox, R.T., 1994, Analysis of drainage basin symmetry as a rapid technique to identify areas of possible Quaternary tilt-block tectonics: An example from the Mississippi Embayment: Geological Society of America Bulletin, v. 106, p. 571-581.

Crone, A.J., and Luza, K.V., 1990, Style and timing of Holocene surface faulting on the Meers fault, southwestern Oklahoma: Geological Society of America Bulletin, v. 102, p. 1-17.

Dillon, W.P., Paull, C.K., Buffler, R.T., and Fail, J.P., 1979, Structure and development of the Southeast Georgia embayment and Northern Blake Plateau-Preliminary analysis: *in* Watkins, J.S., Montadert, L., and Dickerson, P.W., eds., Geological and geophysical investigations of continental margins: American Association of Petroleum Geologists Memoir 29, p. 27-41.

Durá-Gómez, I., 2004, Seismotectonic framework of the Middleton Place-Summerville seismic zone near Charleston, South Carolina [M.S. thesis]: University of South Carolina, Columbia, South Carolina, 150 p.

Dutton, C.E., 1890, The Charleston earthquake of August 31, 1886: U.S. Geological Survey Ninth Annual Report 1887-1888, 528 p.

Garner, J.T., 1998, Re-evaluation of the seismotectonics of the Charleston, South Carolina area [M.S. thesis]: University of South Carolina, Columbia, South Carolina, 250 p.

Gohn, G.S., 1988, Late Mesozoic and early Cenozoic geology of the Atlantic Coastal Plain: North Carolina to Florida, *in* Sheridan, R.E., and Grow, J.A., eds., The Atlantic Continental Margin, U.S.: Boulder, Colorado, Geological Society of America, Geology of North America, v. I-2, p. 107-130.

Gohn, G.S., Houser, B.B., and Schneider, R.R., 1983, Geology of the lower Mesozoic(?) sedimentary rocks in Clubhouse Crossroads test hole #3, near Charleston, South Carolina, *in* Gohn, G.S., ed., Studies related to the Charleston, South Carolina, earthquake of 1886—Tectonics and seismicity: U.S. Geological Survey Professional Paper 1313-D, 17 p.

Guccione, M., Marple, R., and Autin, W., 2005, Evidence for Holocene displacements along the Bootheel fault (lineament) in southeastern Missouri: Seismotectonic implications for the New Madrid region: Geological Society of America Bulletin, v. 117, no. 3/4, p. 319-333.

Hamilton, R.M., Behrendt, J.C., and Ackermann, H.D., 1983, Land multichannel seismic reflection evidence for tectonic features near Charleston, South Carolina, *in* Gohn, G.S., ed., Studies related to the Charleston, South Carolina, earthquake of 1886—Tectonics and seismicity: U.S. Geological Survey Professional Paper 1313-I, 18 p.

Harding, T.P., 1985, Seismic characteristics and identification of negative flower structures, positive flower structures, and positive structural inversion: The American Association of Petroleum Geologists Bulletin, v. 69, no. 4, p. 582-600.

Hatcher, R.D., Jr., Howell, D.E., and Talwani, P., 1977, Eastern Piedmont fault system: Speculations on its extent: Geology, v. 5, p. 636-640.

Hudnut, K.W., Seeber, L., and Pacheo, J., 1989, Cross-fault triggering in the November 1987 Superstition Hills earthquake sequence, southern California: Geophysical Research Letters, v. 16, p. 199-202.

Johnston, A.C., 1996, Seismic moment assessment of earthquakes in stable continental regions—III. New Madrid 1811-1812, Charleston 1886 and Lisbon 1755: Geophysical Journal International, v. 126, p. 314-344.

Johnston, A.C., Reinbold, D.J., and Brewer, S.I., 1985, Seismotectonics of the southern Appalachians: Seismological Society of America Bulletin, v. 75, p. 291-312.

Kahle, J.E., Wills, C.J., Hart, E.W., Treiman, J.A., Greenwood, R.B., and Kaumeyer, R.S., 1988, Surface rupture; Superstition Hills earthquakes of November 23 and 24, 1987, Imperial County, California: California Geology, v. 41, no. 4, p. 75-84.

King, E.R., and Zietz, I., 1978, The New York-Alabama lineament: Geophysical evidence for a major crustal break in the basement beneath the Appalachian basin: Geology, v. 6, p. 312-318.

King, G., and Nabelek, J., 1985, Role of fault bends in the initiation and termination of earthquake rupture: Science, v. 228, p. 984-987.

Klitgord, K.D., Hutchinson, D.R., and Schouten, H., 1988, U.S. Atlantic continental margin; Structural and tectonic framework: *in* Sheridan, R.E., and Grow, J.A., eds., The Atlantic continental margin, U.S.: Boulder, Colorado, Geological Society of America, Geology of North America, v. I-2, p. 19-55.

Lennon, G., 1986, Identification of a northwest trending seismogenic graben near Charleston, South Carolina: U.S. Nuclear Regulatory Commission Report NUREG/CR-4705, p. 1-43.

Machette, M.N., Crone, A.J., and Bowman, J.R., 1993, Geologic investigations of the 1986 Marryat Creek, Australia, earthquake-Implications for paleoseismicity in stable continental regions: U.S. Geological Survey Bulletin 2032-B, 29 p.

Madabhushi, S., and Talwani, P., 1993, Fault plane solutions and relocations of recent earthquakes in Middleton Place-Summerville seismic zone near Charleston, South Carolina: Bulletin of the Seismological Society of America, v. 83, no. 5, p. 1442-1466.

Marple, R.T., 1994, Discovery of a possible seismogenic fault system beneath the Coastal Plain of South and

North Carolina from an integration of river morphology and geological and geophysical data [Ph.D. dissert.]: Columbia, University of South Carolina, 354 p., 13 plates.

Marple, R.T., and Talwani, P., 1993, Evidence of possible tectonic upwarping along the South Carolina Coastal Plain from an examination of river morphology and elevation data: Geology, v. 21, no. 7, p. 651-654.

Marple, R.T., and Talwani, P., 2000, Evidence for a buried fault system in the Coastal Plain of the Carolinas and Virginia—Implications for neotectonics in the southeastern United States: Geological Society of America Bulletin, v. 112, no. 2, p. 200-220.

Marple, R.T., and Talwani, P., 2004, Proposed Shenandoah fault and East Coast-Stafford fault system and their implications for eastern U.S. tectonics: Southeastern Geology, v. 43, no. 2, p. 57-80.

Marple, R.T., and Talwani, P., 2006, Possible connection between the East Coast-Stafford fault system and Norumbega fault zone in southern New England: Northeastern Geology and Environmental Sciences, v. 28, no. 3, p. 215-230.

Miller, R.D., Pullan, S.E., Steeples, D.W., and Hunter, J.A., 1992, Field comparison of shallow seismic sources near Chino, California: Geophysics, v. 57, p. 693-709.

Naylor, M.A., Mandl, G., and Sijpesteijn, C.H.K., 1986, Fault geometries in basement-induced wrench faulting under different initial stress states: Journal of Structural Geology, v. 8, no. 7, p. 737-752.

Nuttli, O.W., Bollinger, G.A., and Herrmann, R.B., 1986, The 1886 Charleston, South Carolina, Earthquake—A 1986 perspective: U.S. Geological Survey Circular 985, 52 p.

Pazzaglia, F.J., 1993, Stratigraphy, petrography, and correlation of late Cenozoic middle Atlantic Coastal Plain deposits: Implications for late-state passive-margin geologic evolution: Geological Society of America Bulletin, v. 105, p. 1617-1634.

Peters, K.E., and Herrmann, R.B., eds., 1986, First-hand observations of the Charleston Earthquake of August 31, 1886, and other earthquake materials: Reports of WJ McGee, Earle Sloan, Gabriel E. Manigault, Simon Newcomb, and Others: South Carolina Geological Survey Bulletin 41, 116 p.

Phillips, J.D., 1988, Buried structures at the northern end of the early Mesozoic South Georgia basin, South Carolina, as interpreted from aeromagnetic data, *in* Froelich, A.J., and Robinson, G.R., eds., Studies of the early Mesozoic basins of the eastern United States: U.S. Geological Survey Bulletin 1776, p. 248-252.

Poley, C.M., and Talwani, P., 1986, Recent vertical crustal movements near Charleston, South Carolina: Journal of Geophysical Research, v. 91, p. 9056-9066.

Schilt, F.S., Brown, L.D., Oliver, J.E., and Kaufman, S., 1983, Subsurface structure near Charleston, South Carolina—Results of COCORP reflection profiling in the Atlantic Coastal Plain, *in* Gohn, G.S., ed., Studies related to the Charleston, South Carolina, earthquake of 1886—Tectonics and seismicity: U.S. Geological Survey Professional Paper 1313-H, 19 p.

Seeber, L., and Armbruster, J.G., 1981, The 1886 Charleston, South Carolina earthquake and the Appalachian décollement: Journal of Geophysical Research, v. 86, no. B9, p. 7874-7894.

Sibson, R.H., 1990, Rupture nucleation on unfavorably oriented faults: Bulletin of the Seismological Society of America, v. 80, p. 1580-1604.

Soller, D.R., 1988, Geology and tectonic history of the lower Cape Fear River valley, southeastern North Carolina: U.S. Geological Survey Professional Paper 1466-A, 60 p.

Talwani, P., 1986, Seismotectonics of the Charleston region, *in* Proceedings of the Third U.S. National Conference on Earthquake Engineering: Earthquake Engineering Research Institute, v. 1, p. 15-24.

Talwani, P., 1999, Fault geometry and earthquakes in continental interiors: Tectonophysics, v. 305, p. 371-379.

Tucker, P.M., and Yorston, H.J., 1973, Pitfalls in seismic interpretation, *in* Wenschel, P.C., ed., Society of Exploration Geophysicists, Monograph Series Number 2, 50 p.

Wald, D.J., Helmberger, D.V., and Hartzell, S.H., 1990, Rupture process of the 1987 Superstition Hills earthquake from the inversion of strong-motion data: Bulletin of the Seismological Society of America, v. 80, no. 5, p. 1079-1098.

Wallace, R.E., 1990, The San Andreas fault system, ed., U.S. Geological Survey Professional Paper 1515, 279 p.

Weems, R.E., and Lemon, E.M., Jr., 1988, Geologic map of the Ladson quadrangle, Berkeley, Charleston, and Dorchester counties, South Carolina: U.S. Geological Survey Geologic Quadrangle Map GQ-1630, scale 1:24,000, text.

Weems, R.E., and Lewis, W.C., 2002, Structural and tectonic setting of the Charleston, South Carolina, region: Evidence from the Tertiary stratigraphic record: Geological Society of America Bulletin: v. 114, no. 1, p. 24-42.

Weems, R.E., Lemon, E.M., Jr., and Nelson, M.O., 1997, Geologic map of the Pringletown, Ridgeville, Summerville, and Summerville Northwest 7.5-minute quadrangles, Berkeley, Charleston, and Dorchester Counties, South Carolina: U.S. Geological Survey Miscellaneous Investigations Map I-2502, scale 1:24,000, 2 sheets, 9 p.

Yantis, B.R., Costain, J.K., and Ackermann, H.D., 1983, A reflection seismic study near Charleston, South Carolina, *in* Gohn, G.S., ed., Studies related to the Charleston, South Carolina, earthquake of 1886—Tectonics and seismicity: U.S. Geological Survey Professional Paper 1313-G, 20 p.

Zoback, M.L., and Zoback, M.D., 1989, Tectonic stress field of the continental United States: *in* Pakiser, L.C., and Mooney, W.D., eds., Geophysical framework of the continental United States: Boulder, Colorado, Geological Society of America Memoir 172, p. 523-539.

SOUTHEASTERN GEOLOGY
V. 44, No. 3, October 2006, p. 129-135

MORPHOLOGY OF THE LARGE CENOZOIC SPATANGOID ECHINOID *BRISSUS* GRAY FROM NORTH AND SOUTH CAROLINA

DAVID N. LEWIS

Department of Palaeontology
The Natural History Museum
Cromwell Road, London, SW7 5BD
England
dnl@nhm.ac.uk

STEPHEN K. DONOVAN

Department of Geology
Nationaal Natuurhistorisch Museum
Postbus 9517, 2300 RA Leiden
The Netherlands
Donovan@naturalis.nnm.nl

DON CLEMENTS

67 South Hummingbird Lane
Rocky Point
North Carolina 28457
Abborean@aol.com

ABSTRACT

Large spatangoid echinoids with thin tests have a poor Neogene fossil record. *Brissus glenni* Cooke (Upper? Miocene) was described from a unique, poorly preserved specimen lacking the oral surface; the peripetalous fasciole has a similar geometry to the type species, *Brissus unicolor* (Leske). A complete test, *Brissus glenni*? (Plio-Pleistocene), preserves the oral surface, but has lost surface details (fascioles and other tuberculation) removed by cleaning. The anterior petals and gross morphology are not identical to *B. glenni sensu stricto*, but it is uncertain if such differences are intraspecific or interspecific. It is uncertain if brissid sp. indet. (Plio-Pleistocene) is congeneric; it may be *Meoma*. It was crushed post-burial, but pre-cementation, and its features are thus disrupted; it is also concealed by encrusting invertebrates, indicating a finite residence time on the sea floor, and by obdurate lithified clasts. Unlike the other specimens considered herein, it preserves the sub-anal fasciole.

INTRODUCTION

Among the many species of fossil echinoid described therein, Cooke (1959, p. 82, pl. 36, figs 5, 6; Fig. 1 herein) erected the Upper Miocene(?) spatangoid (heart urchin) *Brissus glenni* on the basis of a single, poorly preserved specimen which does not retain the oral surface. Although incompletely known, this species is nevertheless of some interest, being a rare example of a nominal species of large spatangoid echinoid from the Neogene of the Carolinas. The prevalence of smaller over larger Cenozoic echinoids in coeval deposits was discussed by Donovan and Clements (2002). Apart from the clypeasteroids, a group with robust tests, complete large fossil echinoid tests are rare from the Neogene of the southeast USA and Caribbean. Fragments of tests of large, spatangoid echinoids, identifiable in only broad terms (e.g., spatangoid sp. indet.), occur only locally. The taphonomic pathways leading to such a pattern were discussed by Donovan and Clements (2002).

It is therefore of some interest to report two further specimens of large, fossil spatangoid echinoid from the Carolinas that may be conspecific or, at least, related to *B. glenni*. Both specimens preserve the oral surface, adding to their potential value and interest. Although both are sufficiently poorly preserved to necessitate caution in their specific assignment, they nevertheless provide new data on the morphology of a group of fossils that remain poorly known and documented, yet, by comparison with modern environments, must have been important members of the benthos (e.g., Hendler et al., 1995).

The terminology of the echinoid endoskeleton used herein follows Melville and Durham (1966), Durham and Wagner (1966) and Smith (1984). Our philosophy of open nomenclature follows Bengtson (1988). The sequential description of each specimen follows Lewis & Donovan (2007), organized to satisfy the format of this journal. Specimens discussed herein are deposited in the Nationaal Natuurhistorisch Museum, Leiden (NNM RGM, the latter being an abbreviation of Rijksmuseum van Geologie en Mineralogie; Brongersma, 1978) and the National Museum of Natural History, Smithsonian Institution, Washington, D.C. (USNM).

SYSTEMATIC PALEONTOLOGY

Class ECHINOIDEA Leske
Superorder NEOGNATHOSTOMATA Smith
Order SPATANGOIDA Claus
Family BRISSIDAE Gray
Genus *Brissus* Gray

Type species. – *Spatangus brissus unicolor* Leske, 1778, p. 248, by the subsequent designation of the International Commission on Zoological Nomenclature (1954, p. 387) (Fischer, 1966, p. U582).

Diagnosis. – (After Donovan and Veale, 1996, p. 635). "Test elongate ovoid in outline, moderate to large as adult. Test more or less highly arched aborally; posterior interambulacrum may be raised as a keel. Oral surface flattened to gently convex. Anterior sinus not developed, posterior truncate. Apical system anterior, ethmolytic (Smith, 1984, fig. 3.22), with 4 genital pores (genital 5 absent); posterior pores larger than anterior. Anterior ambulacrum narrow, not petaloid. Paired ambulacral petals sunken; anterior petals approximately transverse, posterior petals not widely divergent. First plate of interambulacrum 1 followed by single plate. Plastron large, ultraamphisterous. Peripetalous and subanal fascioles developed; subanal fasciole broad with lateral lobes. Periproct lenticular in outline, on upper part of truncate posterior margin. Peristome near anterior, semilunate, with broad, but not prominent, labrum; conspicuous phyllodes developed. Tuberculation dense. Pedicellariae usually of five types; globiferous, tridentate, rostrate, ophicephalous and triphyllous."

Range. – Eocene to Recent (Fischer, 1966, p. U583)

Brissus glenni Cooke

(Figure 1)

1959 *Brissus glenni* n. sp. – Cooke, p. 82, pl. 36, figs 5, 6.

Holotype. – Holotype, USNM 562451, moderately well preserved apart from the absence of the oral surface. Other specimens unknown.

Locality and horizon. – "South Carolina: Intracoastal Waterway canal in Horry County 1 to 1½ miles southwest of the bridge on US 17 near Nixons Crossroads, about 15 miles northeast of Myrtle Beach (USGS 18759, L. C. Glenn)... Probably late Miocene" (Cooke, 1959, p. 82).

Description. – See Cooke (1959, p. 82).

Measurements. – (Abbreviations following Donovan and Veale, 1996.) Test length (TL) = > 107.5 mm; test width (TW) = estimated > 86.5 mm; test height (TH) = estimated > 47.0 mm; distance from apical system to anterior (AA) = c. 12.5 mm; length of petal V (Lv) = c. 67.0 mm; length of petal IV (Liv) = c. 48.0 mm; number of pore pairs in outer half ambulacrum of petal V (Ppv) = 40; number of pore pairs in anterior half ambulacrum of petal IV (Ppiv) = estimated 37.

Discussion. – The holotype of Cooke's *B. glenni* is large and impressive in apical view, but with that part of the test below the ambitus missing (Cooke, 1959, pl. 36, fig. 6; Fig. 1b

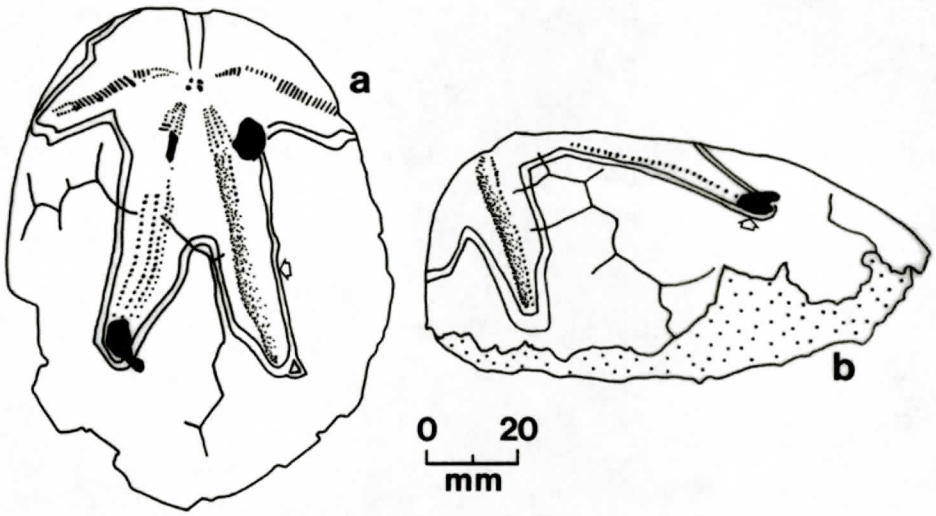

Figure 1. *Brissus glenni* Cooke, 1959, holotype, USNM 562451, drawings taken from photographic illustrations in Cooke (1959, pl. 36, figs 5, 6, respectively), and with the position and morphology of the peripetalous fasciole emphasized (arrows) by reference to the specimen. a, apical view. Peripetalous fasciole not preserved anterior and right. b, left lateral view. Specimen not preserved below the ambitus; coarse stipple = sedimentary infill.

herein). Cooke (1959, p. 82) noted that "Peripetalous fasciole deeply reentrant," although this was only poorly apparent on the plate; it is shown in greater detail herein (Fig. 1). This feature is reminiscent of the type species (Smith and Stockley, 2005, fig. 1). What can be seen of the aboral surface of *B. glenni* compares well with the specimen discussed below.

Brissus glenni? Cooke

(Figure 2)

Material. – One specimen, NNM RGM 211 448, a complete test, very polished so that there is no fine detail preserved.

Locality and horizon. – Plio-Pleistocene, Upper Waccamaw Formation (Edwards et al., 1997), Little River, Horry County, South Carolina. Collected by Rebecca Clements c.1996, prepared by Del Szatmary and donated to the NNM by Don Clements.

Description. – Test irregular, elongated, oval, width 80% of the length, broadly rounded anteriorly, less so posteriorly (Fig. 2a, b); no anteal sulcus; test tall and inflated; oral surface rounded; ambitus rounded; posterior end sloping at about 85° from the apical surface inwards towards the oral surface; anterior end almost flat, sloping at about 60° from the apical surface outwards towards the oral surface (Fig. 2e).

Apical disc anterior, about 25 mm from the anterior end and angled slightly anterior of horizontal. No other details preserved.

Peristome anterior, C-shaped, approximately 18 mm wide and with well defined labrum, about 15 mm from the anterior margin and overhanging to form the C-shaped peristome (Fig. 2b, d).

Periproct at posterior end, oval, vertically elongated, 16 mm tall x 10 mm wide (Fig. 2c).

Apical ambulacra petaloid, with narrow petals, closed at ends, not reaching ambitus; no anterior ambulacral petal defined; anterior petals 38 mm long, up to 6 mm wide; posterior petals c. 45 mm long, up to 6 mm wide. Petals deeply sunken, with anterior pair reflexed ad-anteriorly about a third of the way from the ends; posterior pair only slightly curved away from the posterior end. Anterior pair about 30 mm from the anterior end and about 10 mm from the ambitus; ends of posterior pair about 30 mm from the

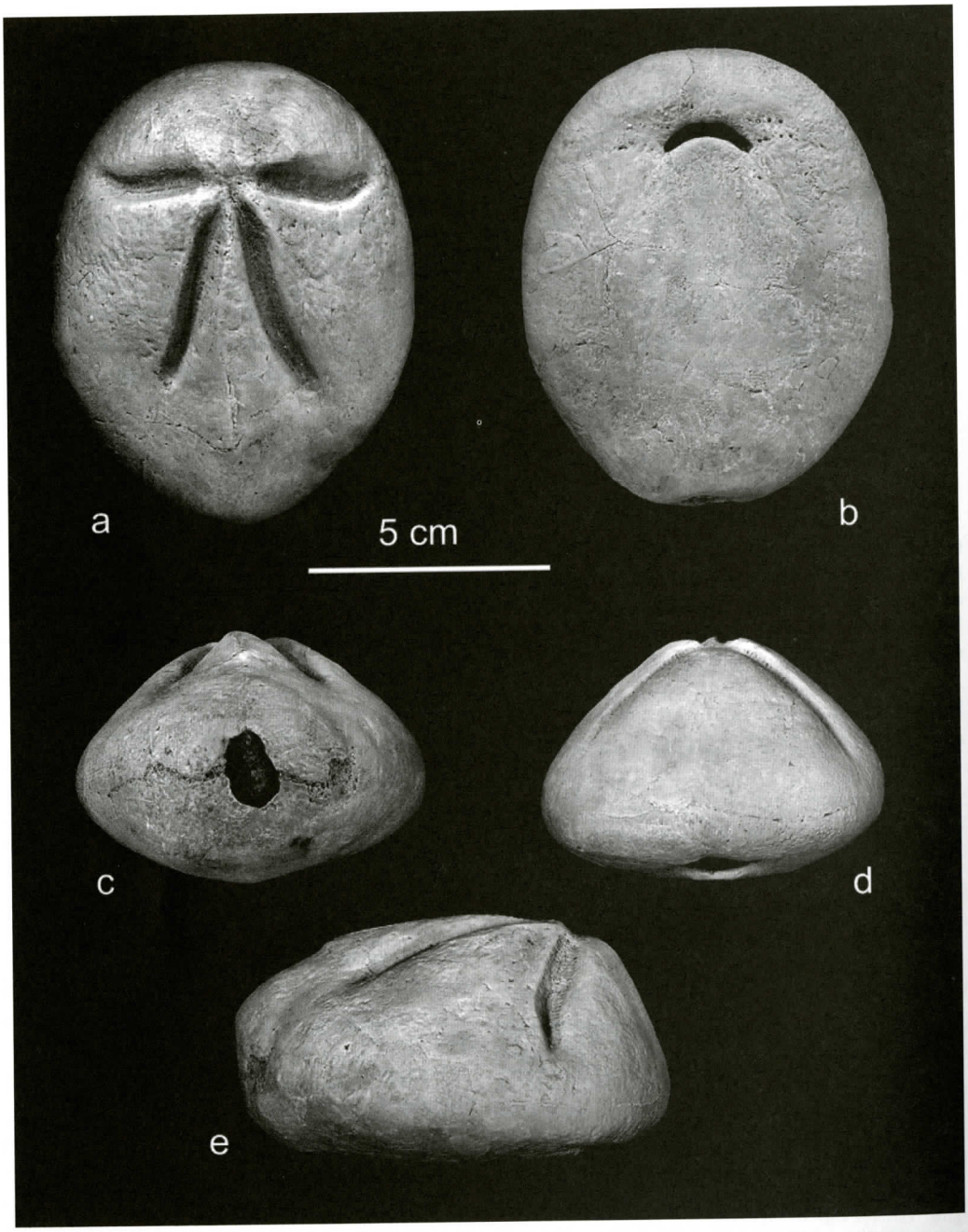

Figure 2. *Brissus glenni*? Cooke, 1959, NNM RGM 211 448, Plio-Pleistocene, Upper Waccamaw Formation, Little River, Horry County, South Carolina. a, apical view. b, oral surface. c, posterior view. d, anterior view. e, right lateral view. Specimen coated with ammonium chloride.

posterior margin of the ambitus; pore pairs straight, non-conjugate, perradial pore teardrop shaped, adradial pore more elongate teardrop shaped; pore columns simple; about 40 pore pairs per posterior petal, 33-35 pore pairs per anterior petal. Buccal pores large and appearing single.

Interambulacra very wide, with weathered

traces of small, evenly distributed tubercles in regular series; sternal plate configuration unclear.

Fascioles not preserved.

Measurements. – (Abbreviations following Donovan and Veale, 1996, and as above.) TL = 98.0 mm; TW = 79.0 mm; TH = 55.5 mm; test height at apical system (Tha) = 50.1 mm; AA = c. 26.0 mm; Lv = 39.8 mm; Liv = 33.6 mm; Ppv = 37+; Ppiv = 35; periproct height (PH) = 15.7 mm; periproct width (PW) = 10.8 mm.

Discussion. – This specimen is close in gross morphology to *B. glenni*, but is not identical and lacks important morphological features, hence its tentative identification. The test of RGM 211 448 is more rounded anteriorly and is widest more anteriorly than USNM 562451. The anterior paired petals of *B. glenni* curve forwards immediately adjacent to the apical system, but are thereafter straight and directed slightly anteriorly. In contrast, *B. glenni*? has anterior paired petals that are straight more apically, but angled slightly posteriorly, curving anteriorly towards the tips. Without a larger suite of more well-preserved samples, it is impossible to determine if these differences are interspecific or intraspecific.

Brissid sp. indet.

(Figure 3)

Material. – One specimen, RGM 211 449, an almost complete, but crushed and fragmented test, with cemented sand grains over much of the surface. The distortion is such that overall dimensions are approximate.

Locality and horizon. – Plio-Pleistocene, Lower Waccamaw Formation, Shallotte, Brunswick County, North Carolina. Collected by Don Clements c. 1994 and donated to the NNM.

Description. – Test large, irregular in shape, elongated, oval, width 80% of the length (Fig. 3a, b); no anteal sulcus; test tall; oral surface rounded; ambitus rounded; posterior end sloping, but too crushed to determine degree of slope; anterior end displaced and crushed. Maximum height of test apparently towards the posterior end (Fig. 3c).

Apical disc missing; position anterior, about 36 mm from the anterior end.

Peristome anterior, C-shaped, approximately 9 mm wide and with well defined labrum, about 22 mm from the anterior margin and overhanging to form the C-shaped peristome (Fig. 3b).

Periproct at posterior end, oval, vertically elongated, approximately 17 mm tall x 13 mm wide.

Apical ambulacra petaloid, with narrow petals, closed at ends, not reaching ambitus; no anterior ambulacral petal defined; anterior petals c. 42 mm long, up to 7 mm wide; posterior petals c. 44 mm long, up to 8 mm wide. Petals are deeply sunken, with anterior pair gently curved towards anterior; posterior pair only slightly curved away from the posterior end and III-5 axis. Anterior pair about 30 mm from the anterior end and about 10 mm from the ambitus; ends of posterior pair about 35 mm from the posterior margin of the ambitus; pore pairs straight, non-conjugate, both pores of a pair tear-drop shaped; about 31 pore pairs per posterior column, 27 pore pairs per anterior column. Oral pores large and single.

Interambulacra very wide, with weathered traces of small, evenly distributed tubercles in regular series. The interambulacral tubercles are small, closely spaced and evenly distributed over the apical surface. Those of the anterior interambulacra are twice the size of the rest. On the oral surface the anterior tubercles are larger anteriorly and gradually become smaller posterior-wards, those on the plastron are arranged in a regular pattern. The plastron is ultramphisternous.

Sub-anal and peripetalous fascioles present. Sub-anal fasciole kidney-shaped. The peripetalous fasciole is deeply indented, following the outline of the petals.

Measurements. – (Abbreviations as above.) TL = c. 110.0 mm; TW = c. 91.6 mm; TH = at least 58.0 mm; Tha = c. 48.1 mm; Lv = 39.8+ mm (petal incomplete); Liv = 30.1+ mm; Ppv = 31+; other parameters unmeasurable.

Discussion. – This test has been crushed and disrupted with many cracks that do not follow the plate boundaries. This pattern of breakage surely could only have occurred after final burial, but before pervasive cementation (compare with Donovan and Clements, 2002). The anteri-

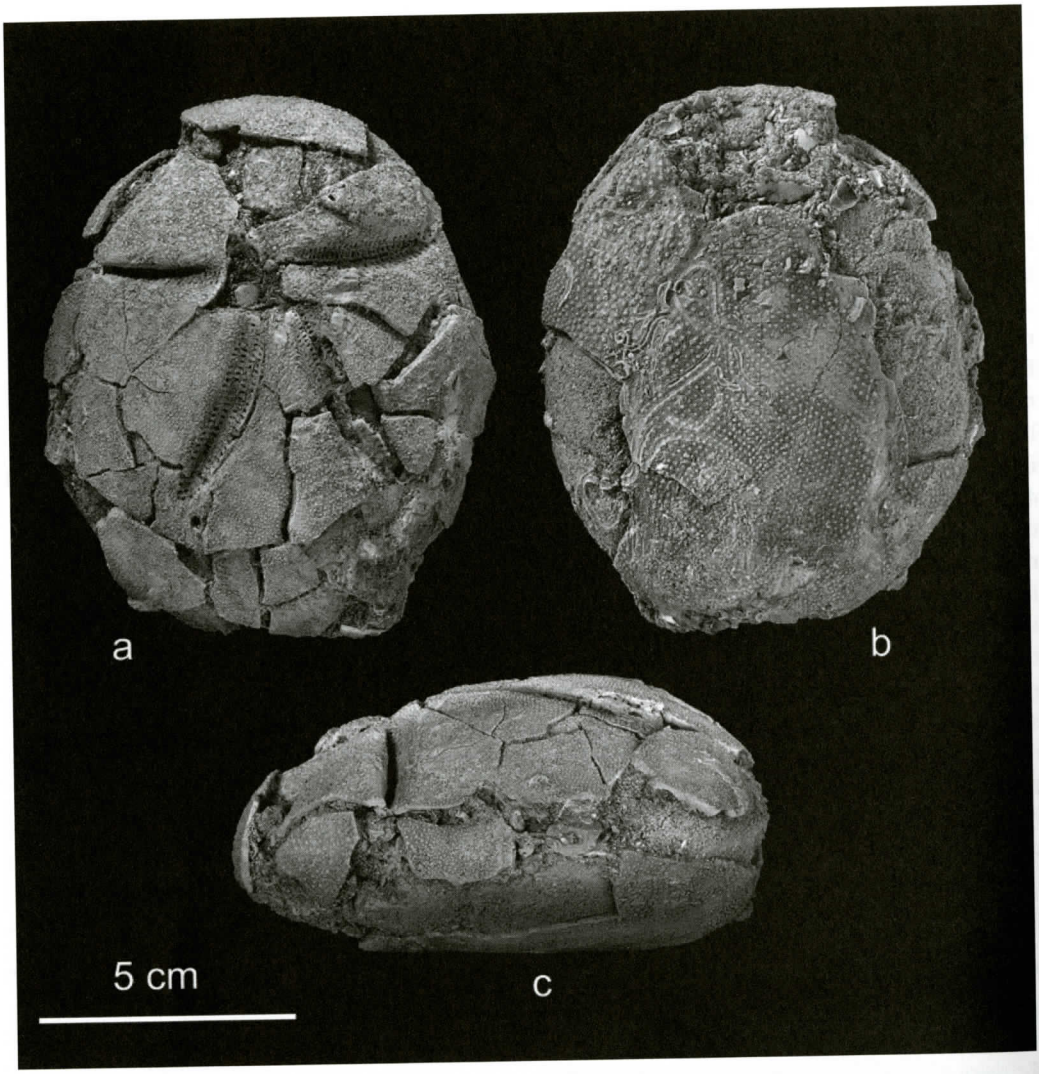

Figure 3. Brissid sp. indet., NNM RGM 211 449, Plio-Pleistocene, Lower Waccamaw Formation, Shallotte, Brunswick County, North Carolina. a, apical view. b, oral surface. c, left lateral view. Specimen coated with ammonium chloride.

or paired petals are essentially straight and not close to either specimen discussed above, although possibly resembling the RGM specimen more; however, the poor state of preservation makes any comparison speculative. Where apparent, the peripetalous fasciole follows a similar track to *B. glenni*. The test, although cleaned by light air abrasion, still retains some particularly obdurate, cemented shell fragments and is obscured, mainly on parts of the oral surface, by bryozoans and serpulid worm tubes, the latter relics of a period of residence on the ancient Waccamaw sea floor before final burial. The sub-anal fasciole, a feature not seen on other specimens considered herein, is poorly seen; it may be similar to that of *Brissus unicolor* (Stockley et al., 2005, fig. 6). However, gross test geometry is also reminiscent of *Meoma* (Dr. A.B. Smith, pers. comm. to S. K. D., April 2006) and it may be that this specimen is considered as an addition to the analysis of Donovan and Clements (2002).

ACKNOWLEDGMENTS

The images in Figures 2 and 3 were taken by the Photographic Unit, The Natural History Museum, London. Access to the holotype of *B. glenni* by S. K. D. was made possible by Jann Thompson (USNM), who is gratefully acknowledged. Adrian Doyle (Palaeontology Conservation Unit, The Natural History Museum, London (BMNH)) kindly cleaned the test of brissid sp. indet. We thank Dr. Andrew Smith (BMNH) for his comments on the figured specimens. Constructive reviews by Professor Burchard Carter (Georgia Southwestern State University, Americus) and Dr. Louis Zachos (Texas Memorial Museum, Austin) are gratefully acknowledged.

REFERENCES CITED

Bengtson, P., 1988, Open nomenclature: Palaeontology, v. 31, p. 223-227.

Brongersma, L. D., 1978, Rijksmuseum van Geologie en Mineralogie 1878-1978: Scripta Geologica, v. 48, p. 37-96.

Cooke, C. W., 1959, Cenozoic echinoids of eastern United States: U. S. Geological Survey Professional Paper, v. 321, p. 1-106, pls 1-43.

Donovan, S. K. and Clements, D., 2002, Taphonomy of large echinoids: *Meoma ventricosa* (Lamarck) from the Pliocene of South Carolina: Southeastern Geology, v. 41, p. 169-176.

Donovan, S. K. and Veale, C., 1996, The irregular echinoids *Echinoneus* Leske and *Brissus* Gray in the Cenozoic of the Antillean region: Journal of Paleontology, v. 70, p. 632-640.

Durham, J. W. and Wagner, C. D., 1966, Glossary of morphological terms applied to echinoids, *in* Treatise on Invertebrate Paleontology, Part U, Echinodermata 3(1), R. C. Moore, ed.: Geological Society of America and University of Kansas Press, New York and Lawrence, p. U251, U253-U256.

Edwards, L. E., Bybell, L. M., Gohn, G. S. and Frederiksen, N. O., 1997, Paleontology and physical stratigraphy of the USGS-Pregnall no. 1 core (DOR-208), Dorchester County, South Carolina: U.S. Geological Survey, Open-file Report, no. 97-145, 35 p.

Fischer, A. G., 1966, Spatangoids, *in* Treatise on Invertebrate Paleontology, Part U, Echinodermata 3(2), R. C. Moore, ed.: Geological Society of America and University of Kansas Press, New York and Lawrence, p. U543-U628.

Hendler, G., Miller, J. E., Pawson, D. L. and Kier, P. M., 1995, Sea Stars, Sea Urchins, and Allies: Echinoderms of Florida and the Caribbean: Smithsonian Institution Press, Washington, D.C., xii+390 p.

International Commission on Zoological Nomenclature, 1954, Opinion 209. Validation of, and designation of type species for, "*Brissus*" Gray, 1825, "*Echinocardium*" Gray, 1825, and "*Spatangus*" Gray, 1825 (Class Echinoidea) under the plenary powers, and designation, under those powers, of a type species for "*Schizaster*" Agassiz (L.), 1836, and, in so far as necessary, for "*Moira*" Agassiz (A.), 1872: Opinions and Declarations Rendered by the International Commission on Zoological Nomenclature, v. 3, p. 367-392.

Leske, N. G., 1778, Iacobi Theodori Klein Naturalis dispositio Echinodermatum, edita et aucta a N.G. Leske: Lipsiae, 278 p. [Not seen.]

Lewis, D. N. and Donovan, S. K., 2007 (in press), Notes on describing fossils, with particular reference to the Echinoidea: Scripta Geologica, v. 134.

Melville, R. V. and Durham, J. W., 1966, Skeletal morphology, *in* Treatise on Invertebrate Paleontology, Part U, Echinodermata 3(1), R. C. Moore, ed.: Geological Society of America and University of Kansas Press, New York and Lawrence, p. U220-U251.

Smith, A. B., 1984, Echinoid Palaeobiology: George Allen & Unwin, London, xii+191 p.

Smith, A. B. and Stockley, B., 2005, Fasciole pathways in spatangoid echinoids: a new source of phylogenetically informative characters: Zoological Journal of the Linnean Society, v. 144, p. 15-35.

Stockley, B., Smith, A. B., Littlewood, D. T. J., Lessios, H. A. and MacKenzie-Dodds, J. A., 2005, Phylogenetic relationships of spatangoid sea urchins (Echinoidea): taxon sampling density and congruence between morphological and molecular estimates: Zoologica Scripta, v. 34, p. 447-468.

SOUTHEASTERN GEOLOGY
V. 44, No. 3, October 2006, p. 137-145

IRON MOUNTAIN, SANTA ROSA COUNTY, FLORIDA: A PALEOGROUNDWATER TABLE INVERTED RELIEF FEATURE

CARL R. FROEDE JR.

United States Environmental Protection Agency
Region 4
61 Forsyth Street
Atlanta, GA 30303-8960

BRIAN R. RUCKER

Pensacola Junior College, Warrington Campus
Arts & Sciences Department
5555 West Highway 98
Pensacola, FL 32507-1097

ABSTRACT

Iron Mountain is a small, isolated butte located in north central Santa Rosa County, Florida. Its ascending stratigraphic profile within the undifferentiated Citronelle Formation (Upper Pliocene) reflects a sea level regression from estuarine and lagoonal silts and clays to nearshore marginal marine quartz-sands. Superimposed on the upper few meters of the section is a lateritic profile capped by an iron oxide ferricrete. The laterite layer did not form from top-down soil weathering processes, but rather as a result of the movement of anoxic, acidic groundwater through the subsurface. Sea level withdrawal from the area coincided with the oxidation of the iron-rich groundwater and resulted in the cementation of the quartz sands in the subsurface. The eventual erosion and removal of the overlying Pleistocene siliciclastic sediments subsequently exposed the ferricrete. The uneven lateral coverage provided by the ferricrete cap has contributed to the formation of the Iron Mountain butte. Today, the ferruginized sediment cap has reduced erosion to the underlying silts and clays, and enhanced the development of this topographic feature. Iron Mountain represents the end state in the development of an inverted groundwater table relief feature and is comparable to similar features developed in Australia, India, and Africa.

INTRODUCTION

Since it was first recognized as a formal stratigraphic unit, the sediments of the Citronelle Formation have been interpreted as fluvial-deltaic (Matson, 1916; Berry, 1916). However, within the western Florida panhandle, both Marsh (1966) and Otvos (1998, 2004) identified clay intervals containing the marine trace fossil *Ophiomorpha*. The Citronelle Formation (Upper Pliocene - Scott, 2001) within our study area exhibits an ascending profile reflective of sea level regression documenting the transition from estuarine and lagoonal silts and clays to more nearshore, marginal marine coarse-grained quartz sands.

Pedologists recognize that the intense subaerial weathering of surficial sediments in humid and tropical climates can result in the top-down aqueous transfer and precipitation of various minerals in the shallow subsurface (typically within the vadose zone). This highly weathered soil profile is identified as a laterite (Alexander and Cady, 1962; Maignien, 1966). In some instances, the weathering forms cemented layers in the subsurface which are identified as hardpans. Today, soil scientists classify these ferruginous soils as Oxisols and Ultisols (Buol and others, 1980).

Hydrogeologically, the movement of groundwater within the subsurface can also create laterized sediments (McFarlane, 1976; Twidale, 1984, 1990). Acidic and anoxic

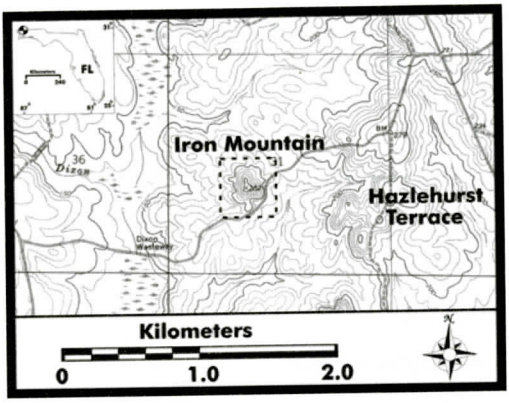

Figure 1. Iron Mountain is located in north central Santa Rosa County, Florida. The isolated feature is covered by a ferricrete cap, which has both protected it from erosion and contributed to its separation from the adjacent Hazlehurst Terrace. The relatively flat-lying surface covers approximately 0.74 hectares and is 16 m above the surrounding landscape. Map constructed from the U.S. Geological Survey 7.5 minute quadrangle for McLellan, FLA.–ALA., 1973, revised 1984. The topographic contour interval is 10 feet.

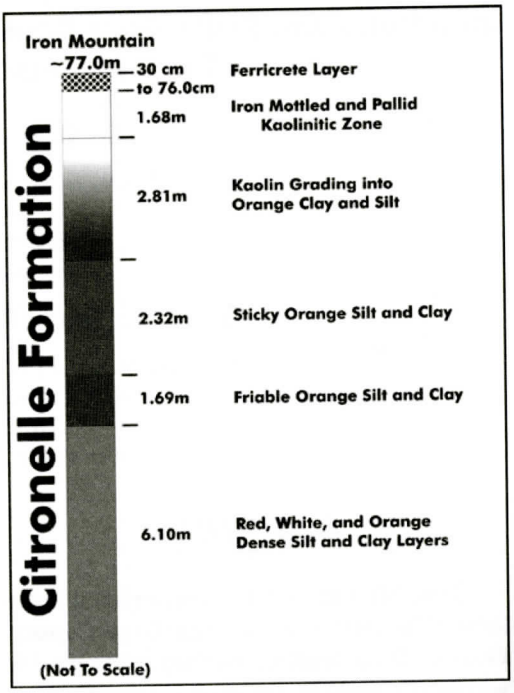

Figure 2. Composite stratigraphic section of Iron Mountain. The ascending sedimentary units reflect an estuarine to lagoonal setting transitioning to an energetic sandy nearshore (a regressive sequence). In association with sea level withdrawal anoxic and acidic groundwater migrated within the subsurface created the weathered "laterite" zone. When the iron-rich groundwater reached an oxidizing environment, iron and other minerals precipitated as cements in the porous and permeable quartz-sand layer, forming the ferricrete cap.

groundwater can both leach and precipitate minerals due to the changing pH and Eh conditions in the subsurface. Iron is especially subject to dissolution, transport, and precipitation under these conditions (Peterson, 1971; Norton, 1973; Mann and Ollier, 1985). Sediments within the zone of groundwater movement and fluctuation can develop a weathered (i.e., leached) lateritic profile totally unrelated to the vertical weathering more typical to soil forming processes. The oxidation of iron-rich groundwater within the subsurface can also create ferruginous hardpan layers more commonly referred to as ferricretes.

Iron Mountain is located in north central Santa Rosa County, Florida [Figure 1]. It was once a part of the adjacent Hazlehurst Terrace. Today, several gullies around the topographic feature provide a composite exposure of the Upper Pliocene, Citronelle Formation (Figure 2). The butte is capped by a ferricrete which overlies a weathered laterite profile beneath which are oxidized silts and clays. We examined Iron Mountain in an attempt to understand its geomorphic setting, stratigraphic history, impact of groundwater laterization, and its eventual development into a groundwater table relief inversion feature.

HISTORY

The first historical record of Iron Mountain stems from the late 1830s. The *Pensacola Gazette* of May 18, 1839, makes reference to the "mountains" in this vicinity of Santa Rosa County (Iron Mountain is the largest and most distinct of several hills in the area). The newspaper report also noted the iron ore in this area. Whether any of the iron was mined commercially is unknown. In recent years, logging ac-

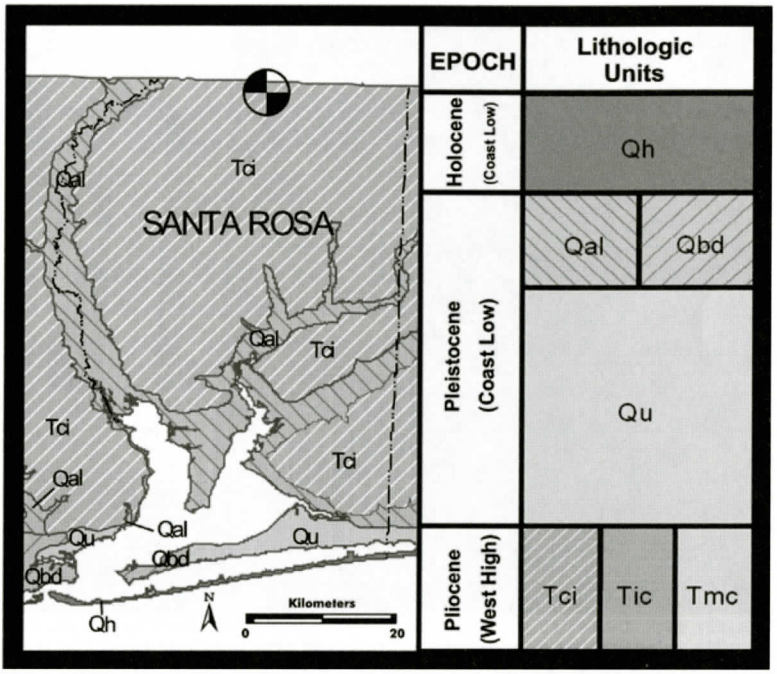

Figure 3. Geologic outcrop map with generalized geomorphic divisions based on the age of the strata. Scott (2005) separates the Western Highlands (West High) from the Gulf Coastal Lowlands (Coast Low) using the 15-meter elevational boundary. Circle indicates location of Iron Mountain.

tivity in the area has contributed to the erosion of the topographic feature. Today, Iron Mountain and the surrounding area are protected from development because they liewithin the Florida Blackwater State Forest.

GEOMORPHIC SETTING

For the Florida panhandle, Cooke (1945) subdivided the Gulf Coastal Plain into the Western Highlands and Coastal Lowlands using the 30-meter elevation as a boundary. Further geomorphic refinement places much of the western panhandle within the Southern Pine Hills District (Means and others, 2000). Scott (2005) proposed unifying the geomorphic divisions in northern Florida with those already in use across the Gulf Coastal Plain. He also reduced the elevational boundary separating the Western Highlands and Coastal Lowlands to the 15-meter contour. Iron Mountain is located in the Western Highlands in Santa Rosa County, Florida (Figure 3). Within the study area, this district is comprised of a series of rolling hills dissected by dendritic drainage generally directed southward toward the Gulf of Mexico.

The retreat of sea level throughout the Neogene has created a series of marine terraces across Florida that progressively drop in elevation as they trend seaward. Matson and Sanford (1913) first noted several of the smaller terraces. Subsequent studies identified additional features which were correlated by elevational similarities (Cooke 1945; MacNeil, 1950; White 1958). Alt and Brooks (1965) questioned this approach and suggested that the proper means of identifying any marine terrace is to trace the relic beach features. They identified five terraces that range in age from late Miocene to Pleistocene (Alt and Brooks, 1965). Today, eight terraces are defined across Florida (Healy, 1975). The development of Iron Mountain can be attributed to the dissection of a portion of the Hazlehurst Terrace, the uppermost marine terrace exposed in northern Santa Rosa County.

Figure 4. Limonitic rhizoliths of a generally consistent size weather from the oxidized silts and clays. The fossilized root casts do not always occur at the same elevation around Iron Mountain.

STRATIGRAPHY AND SEDIMENTOLOGY

Matson (1916) was the first to map and define the Citronelle Formation as a single lithostratigraphic unit that extends across the Gulf Coastal Plain from the western panhandle of Florida to eastern Texas. Berry (1916) identified plant fossils collected from several clay layers near the Citronelle type locality and age-dated them to the Pliocene. The paucity of fossils throughout the lithostratigraphic unit has proven troublesome in identifying the age and paleosetting in which the sediments were deposited (Roy, 1939; Carlston, 1951; Stringfield and LaMoreaux, 1957; Doering, 1958; Isphording and Lamb, 1971). More recently, Scott (1991, 2001) and Otvos (1998, 2004) have assigned the Citronelle Formation to the Upper Pliocene.

The majority of the surficial geology exposed in the Western Highlands of Santa Rosa County is Citronelle Formation (Marsh, 1966; Scott, 1993) [Figure 3]. Marsh (1966) described the Citronelle Formation in Escambia and Santa Rosa Counties as:

> ...principally of quartz sand which contains numerous lenses, beds, and stringers of clay and gravel. The lithology changes abruptly over short distances... The sand is typically light yellowish brown to reddish brown, although some is white or light gray. The grains are mostly angular to subangular and very poorly sorted, ranging from very fine to very coarse. Muscovite is abundant throughout. In places the sand grades into gravel composed of quartz and chert pebbles up to an inch in diameter. Elsewhere the sand grades into siltstone and clay. The siltstone is light gray to light yellow and in places contains abundant carbonized plant remains. The clay occurs in lenses as much as 60 feet thick and is chiefly white or gray, although some is lavender, yellow or brown. Fragments of carbonized wood are common in the gray clay (p. 75-76).

A distinctive rock type that occurs in the Citronelle Formation throughout western Florida and southern Alabama is a limonite-cemented sandstone called

> "hardpan"... This rock, formed by cementation of sand with iron oxides probably precipitated from ground water, is dark rusty brown and is generally extremely hard, although some may be rather soft. The "hardpan" most commonly occurs as layers that parallel the bedding of the enclosed sediments. These layers range from a fraction of an inch to 3 or 4 feet in thickness. Escambia and Santa Rosa counties are dotted with hundreds of ponds, many of which probably owe their existence to "hardpan" layers at or near the surface (p. 77-78).

No gravel lenses were noted at Iron Mountain, an observation that is consistent with Coe's (1979) description of lithology derived from a nearby well core obtained from the top of the Hazlehurst Terrace. A coarse-grained quartz sandstone on top of Iron Mountain is cemented by iron oxide and caps the topographic feature. Directly beneath this ferricrete is a weathered laterite profile consisting of a mottled clay and weathered kaolinitic zone. Beneath this is a transition zone where kaolin decreases and the limonitic silts and clays become much more prevalent. Unweathered silt and clay layers, some of which contain *Ophiomorpha* trace fossils, occur at varying levels within this section. The *Ophiomorpha* traces are consistent in size and orientation with those previously reported in the western Florida panhandle by Marsh (1966) and Otvos (1998, 2004). We also identified several silt and clay intervals that contain rhizoliths. These limonite-cemented plant fossils weather out of some of the lutite layers as small diameter rods (Figure 4).

LATERITES

Buchanan (1807) was the first person to use the term "laterite" to describe iron-rich sedimentary material found within the shallow subsurface that hardened upon oxidation. Over the ensuing years, the variety of soil profiles defined as laterites caused Pullan (1967) to distinguish between lateritic ironstones and ferruginous soils based on their morphology. Since then, the term has further broadened, creating considerable confusion over the definition of what constitutes a laterite profile (Bourman, 1993a; Bourman and Ollier, 2002). We use the term "laterite" in reference to the weathered zone beneath the ferricrete where intense leaching of iron and other materials has created an enriched zone of alumina and silica. This weathered zone is also referred to as the iron mottled and pallid kaolinitic zone (Milnes and others, 1985).

A lateritic profile within a humid tropical setting can contain one or more relatively flat-lying iron-crusts (i.e., ferricretes) above bleached and mottled zones which overlie parent material (Milnes and others, 1985). The iron is believed to be locally derived from either overlying or underlying iron-containing geologic materials (MacFarlane, 1976, Singer, 1975; Bourman and Ollier, 2002). However, this vertical soil weathered profile concept has been challenged, especially where the source of the iron cement could not have been locally derived (Maignien, 1966; Ollier, 1991; Bourman, 1996). The result has been the identification of leached zones and ferricretes in the shallow subsurface created not by soil-forming processes but by anoxic and acidic ferrous groundwater movement within the subsurface (Bourman, 1993b).

The development of laterite in the Citronelle Formation at Iron Mountain can be linked to the diagenetic alteration of formerly saturated sediments. Within this zone, the original clastic materials, bedding, and structures have been completely obliterated (Figure 5). Below the zone of lateritic diagenesis, the now oxidized silts and clays remain relatively unaltered.

An improper understanding of the characteristics of groundwater-formed laterites like this one exhibited at Iron Mountain could lead to confusion in attempting to recreate a potential paleosetting or depositional history for the altered strata. This layer neither formed due to overlying soil weathering nor was it created as part of the original sedimentary setting. Hence, a proper understanding of the original stratigraphy of the area as well as its alteration by groundwater moving within the subsurface is essential to understanding the geological histo-

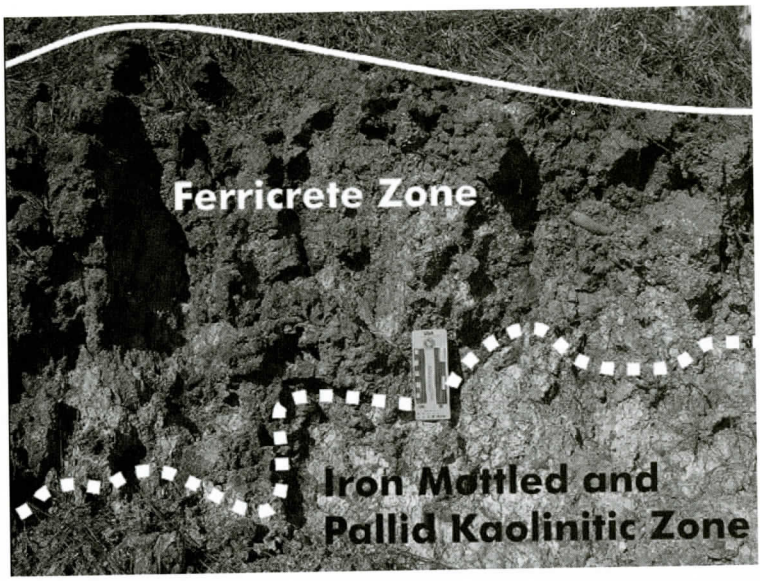

Figure 5. A ferricrete covers an iron mottled and pallid kaolinitic zone. The thickness of the ferricrete varies significantly around the top of Iron Mountain. The original composition, bedding, and structure of the now laterized silts and clays cannot be determined. Additionally, this layer should not be stratigraphically or chronologically correlated to other laterites exposed along the adjacent Hazlehurst Terrace.

ry of the effected sediments. For example, many of the variegated and kaolinitic clays within the Citronelle first described by Cooke and Mossom (1929) formed as a result of groundwater laterization (Coe, 1979). The kaolin is derived from the release of iron and other materials from the limonitic silts and clays (Wright and others, 1992). Additionally, the chronostratigraphic correlation of subsurface laterites and ferricretes across broad areas is not appropriate as these profiles can form at varying times and in different positions within the subsurface (Ollier, 1991; Pain and Ollier, 1992).

FERRICRETE

The term "ferricrete" was first proposed by Lamplugh (1902) to describe the cementation of geologic materials in the shallow subsurface by iron precipitated from groundwater. Perhaps the first reference to iron cement precipitating from emanating groundwater was from Ransome (1901). He reasoned that iron was derived from the weathering of iron sulfides associated with silver ore bodies. The acidic, anoxic and ferrous groundwater entered several creeks within the Silverton Quadrangle (Colorado) and oxidized forming limonite cement (Ransome, 1901).

At Iron Mountain, the ferricrete rests directly on top of a weathered lateritic profile. The source of the iron that created the ferricrete layer was likely derived from local as well as upgradient sources and was transported in the subsurface via groundwater. The ferricrete layer is limited in its lateral extent, which has contributed to the separation of Iron Mountain from the adjacent Hazlehurst Terrace.

Numerous studies have documented the shallow subsurface transport of dissolved iron in groundwater (e.g., Ferguson and others, 1983; Mann and Ollier, 1985; Bourman and others, 1987; Milnes and others, 1987; Wright and others, 1992; Bourman, 1996; Phillips and others, 1997; Furniss and others, 1999; Phillips, 1999; Chan and others, 2000; Phillips, 2000; De Hon and others, 2001; Yager and others, 2003). The movement of acidic and ferrous groundwater under anaerobic conditions precipitates iron

from solution when encountering an oxidizing environment. Although bacteria are recognized as an important component in precipitating iron from groundwater (Aristovskaya, 1974; Fredrickson and others, 1998; Konhauser, 1998; Brown and others, 1999), their role in the formation of ferricretes remains poorly defined.

Currently, ferricrete is recognized in a variety of morphological forms including, ferruginized bedrock, ferruginized sediments, and complex ferricretes (Bourman and others, 1987). In this classification scheme, the ferricrete layer found capping Iron Mountain would be considered a ferruginized sediment as the iron cement has filled the pore spaces between the quartz sand and lithified the sandy convoluted layer into a rock.

INVERTED GROUNDWATER TABLE RELIEF

The terms "inverted relief" and "relief inversion" have been used by geomorphologists to describe a variety of topographically elevated features. While Iron Mountain does not fit the technical definition of an inverted relief feature (i.e., developed from a former valley floor), it is consistent with paleogroundwater table related relief inversion features reported from Africa, India, and Australia (Maignien, 1959; Clare, 1960; Milnes and others, 1985; Ollier and Galloway, 1990; Schwarz, 1994; Pain and Ollier, 1995).

CONCLUSIONS

Undifferentiated clastic sediments of the Citronelle Formation extend across a broad area of the United States Gulf Coastal Plain. Past investigations have suggested that the facies is fluvial to deltaic. However, important recent work has identified additional marine facies that reflect changing sea level positions throughout the Upper Pliocene. Changes in sea level position are also manifested in the development of numerous marine terraces. The Hazlehurst marine terrace in Santa Rosa County, Florida, has been dissected in places creating isolated buttes, many capped by a ferruginized quartz sand.

Laterites have largely been the domain of pedologists. Emphasis has focused primarily on the top-down development of weathered soil profiles and the subsurface development of hardpans. However, site hydrogeologic conditions, along with changes in groundwater chemistry, can also create laterites within the subsurface. Anoxic groundwater moving through the subsurface under changing pH and Eh conditions plays an important role in the diagenetic alteration of subsurface sediments.

We interpret the stratigraphy of Iron Mountain as reflective of a sea level regression during a portion of the Upper Pliocene. A discontinuous quartz sand cover formerly extended across much of the Hazlehurst Terrace in this area above the silt and clay layers. The majority of the iron cement is derived from both local and upgradient source areas and was transported via groundwater. As sea level dropped and the subsurface changed from reducing to oxidizing conditions, the ferrous groundwater precipitated iron oxide within the porous and permeable quartz sands. This formed a ferruginized layer that was later exposed with the removal of the siliciclastic sediment overburden. The armoring provided by the ferricrete cap likely enhanced the dissection of the topographic feature from the Hazlehurst Terrace. Today, Iron Mountain exemplifies an inverted groundwater table relief feature which is comparable to similar features described from Africa, India, and Australia.

ACKNOWLEDGMENTS

We thank A. Jerry Akridge and Eric Brevik for their helpful and constructive comments. Mr. Noah Rucker provided invaluable field assistance. Thajura Harmon-Unongo furnished excellent reference assistance. We are grateful to Ervin Otvos who supplied helpful information about his work on the Citronelle Formation. For the senior author, this work does not necessarily represent the views or opinions of the U.S. Environmental Protection Agency, nor was this investigation conducted in any official capacity. Any mistakes that may remain are the